Biomaterials 335 (2026) 124325

Contents lists available at ScienceDirect

Biomaterials

journal homepage: www.elsevier.com/locate/biomaterials

Additive manufacturing and *in vitro* characterization of scaffolds consisting of PCL/P_2O_5-free bioactive glasses composites with angiogenic and osteogenic potential

Martyna Nikody [a,b,1], Sophia Dalfino [a,c,d,1], Pamela Habibovic [b], Lizette Morejón [e], José A. Delgado [e,f], Gianluca Martino Tartaglia [d,g], Claudia Dolci [c], Elizabeth R. Balmayor [h,*], Lorenzo Moroni [a,**]

[a] Complex Tissue Regeneration, MERLN Institute for Technology-Inspired Regenerative Medicine, Maastricht University, Maastricht, 6229 ER, the Netherlands
[b] Department of Instructive Biomaterials Engineering, MERLN Institute for Technology-Inspired Regenerative Medicine, Maastricht University, Maastricht, the Netherlands
[c] Department of Biomedical Sciences for Health, Università degli Studi di Milano, Milano, Italy
[d] Department of Biomedical, Surgical and Dental Sciences, Università degli Studi di Milano, Milano, Italy
[e] Center of Biomaterials, University of Havana, Havana, 10400, Cuba
[f] Universitat Internacional de Catalunya, Barcelona, 08195, Spain
[g] Fondazione Ca' Granda IRCCS Ospedale Maggiore Policlinico, Milano, Italy
[h] Experimental Orthopaedics and Trauma Surgery, RWTH Aachen University Hospital, Aachen, 52074, Germany

ARTICLE INFO

Keywords:
Bioactive glasses
Composite scaffolds
Osteogenesis
Angiogenesis
Immunomodulation

ABSTRACT

The development of scaffolds with osteogenic and angiogenic properties represents an attractive strategy for regenerating large bone defects. This study describes the fabrication and characterization of bioactive glass-based composite scaffolds for bone regeneration applications. Scaffolds comprising polycaprolactone (PCL) and two different bioactive glasses (BGs), derived from white sand (BG-WS) and yellow sand (BG-YS), at an 80:20 wt% ratio were fabricated with a star-shaped pore geometry. Chemical characterization confirmed the presence of characteristic groups from PCL and BGs. The incorporation of BGs led to increased compressive moduli in the composites compared to PCL scaffolds only. Dissolution products, particularly from PCL/BG-YS, promoted enhanced vascular pattern formation of human umbilical endothelial vein cells (HUVECs) co-cultured indirectly with human mesenchymal stromal cells (hMSCs). Direct culture of hMSCs on PCL/BG-WS and PCL/BG-YS composite scaffolds resulted in greater VEGFA production compared to PCL scaffolds alone. The expression of the early osteogenic marker *RUNX2* was upregulated on day 7 in response to both composite scaffolds, while *ALPL* expression increased only with the PCL/BG-WS scaffolds on day 28. Additionally, late osteogenic gene markers (*COL1A1* and *OCN)* were both upregulated on day 28 in PCL/BG-WS scaffolds. Lastly, the measurement of analytes secreted by hMSCs showed higher secretion levels on day 7 than 28, with PCL scaffolds yielding higher concentrations of IL-10, TNF-α, and CCL2 than composite scaffolds. Overall, both PCL/BG-WS and PCL/BG-YS scaffolds demonstrated osteogenic, angiogenic, and potential immunomodulatory properties. Notably, PCL/BG-WS exhibited the strongest osteogenic responses, which may be attributed to its Ti^{4+} ion content, highlighting the critical role of BG composition in modulating the biological performance of the composites. The findings of this study indicate that combining naturally-derived P_2O_5-free BGs with PCL to fabricate 3D composite scaffolds enhances osteogenic and angiogenic properties of the final constructs, emphasizing their potential in bone regeneration.

* Corresponding author. Professor for Experimental Orthopaedics and Trauma Surgery, RWTH Aachen University Hospital, Pauwelsstraße 30, D-52074 Aachen, Germany.

** Corresponding author. Director MERLN Institute for Technology-Inspired Regenerative Medicine, Chair of Complex Tissue Regeneration Department, Professor in Biofabrication for Regenerative Medicine, Universiteitssingel 40, 6229 ER Maastricht/ Room C3.577, PO Box 616, Maastricht, 6200 MD, the Netherlands.

E-mail addresses: erosadobalma@ukaachen.de (E.R. Balmayor), l.moroni@maastrichtuniversity.nl (L. Moroni).

[1] These authors contributed equally to this work.

https://doi.org/10.1016/j.biomaterials.2026.124325
Received 14 November 2025; Received in revised form 18 May 2026; Accepted 19 May 2026
Available online 20 May 2026
0142-9612/© 2026 The Authors. Published by Elsevier Ltd. This is an open access article under the CC BY license (http://creativecommons.org/licenses/by/4.0/).

1. Introduction

The continuing ageing of the population together with an increasing occurrence of diseases affecting the skeletal system stimulates the research and development of new implantable materials [1]. Nevertheless, bone grafting using native tissue remains the gold standard treatment in the clinical setting [2]. However, autologous or allogenic grafts present several drawbacks, including limited tissue availability, surgical invasiveness, and donor-site morbidity [3].

The field of bone tissue engineering (BTE) aims to address these limitations by developing porous scaffolds, that can support, guide, and enhance the formation of new bone tissue. To effectively mimic the native bone, scaffolds are carefully designed to possess suitable chemical, morphological, and mechanical properties [4]. Melt extrusion-based additive manufacturing (AM), based on a layer-by-layer deposition process, has emerged as an effective method to fabricate porous scaffolds with precise control over their architecture [4]. This technique accommodates a wide range of materials, including biocompatible and biodegradable thermoplastics such as polycaprolactone (PCL) and polylactic acid (PLA), which provide favorable mechanical properties and support long-term tissue growth [4]. These polymers can be combined with inorganic materials to better recapitulate the composition of native bone and enhance osteogenic activity [5].

However, promoting angiogenesis within engineered constructs remains a challenge that needs to be addressed in order to prevent implant failure [6]. To this end, research has focused on the addition of pro-angiogenic cues promoting vascularization into the composites such as bioactive molecules [7], inorganic ions [8], or bioactive glasses (BGs) [9,10].

BGs are a class of amorphous ceramic materials that have been used in the field of bone regeneration for their pro-angiogenic properties [11]. BGs are generally categorized into silicate-based, phosphate--based, and borate-based classes [12], with properties tunable by varying their chemical composition or by adding or removing functional elements like phosphorus, copper, or strontium [13]. The majority of the mainstream BGs contain P_2O_5 in their composition as a source of phosphate groups that participate in hydroxyapatite formation [12,14]. However, studies have shown that the presence of phosphorus can increase the susceptibility of the glass network to hydrolysis. This effect is associated with the formation of P–O–P and P–O–Si bonds, which are more easily cleaved in aqueous environment, resulting in accelerated ion release, uncontrolled dissolution, and faster loss of mechanical integrity [15–17]. A more rapid dissolution can compromise mechanical stability and shorten the time of biological effectiveness, representing undesirable features for bone tissue engineering applications that require a gradual degradation rate. In contrast, BG formulations without P_2O_5 exhibit enhanced chemical durability and more predictable dissolution behavior due to absence of easily hydrolyzed P–O–P and P–O–Si bonds, contributing to a more stable and sustained bioactive response [15–17]. Importantly, several studies have shown that, despite the absence of P_2O_5, such BGs are still capable of apatite formation under physiological conditions and can stimulate biological processes involved in bone regeneration through the controlled delivery of Si^{4+}, Ca^{2+}, as well as trace element ions [18–20]. These properties make P_2O_5-free glasses particularly suitable for applications requiring controlled degradation rates and sustained release of bioactive ions, such as bone defect repair and regeneration [17,20,21]. Specifically, novel P_2O_5-free BGs from the SiO_2–CaO–Na_2O system, synthesized from calcite minerals and silica sands, extracted from natural deposits, have demonstrated promising osteogenic and angiogenic capabilities [18,19]. Among these BG formulations, BG-WS and BG-YS exhibited the most promising biological performance [18]. BG-WS and BG-YS were synthesized from natural raw materials, including calcite and silica sands extracted at different depths of the sand deposit, which influenced both the colour and composition of the silica sands [22]. Specifically, BG-WS was obtained using white silica sand collected from shallower layers of the deposit, while BG-YS originated from yellow silica sand extracted from deeper layers These depth-related differences translated into distinct trace element profiles: BG-WS contained a higher amount of titanium (Ti^{4+}) ions, while BG-YS had more aluminum (Al^{3+}) and iron (Fe^{3+}) ions [22]. Both BG formulations have influenced osteogenic and angiogenic properties, with BG-YS being more potent at influencing osteogenic and angiogenic properties on a gene level, while BG-WS exerted a pronounced effect on vascularization in a CAM assay [18].

In this study, PCL was chosen as the polymeric component of the composite due to its biocompatibility, biodegradability, relatively high mechanical properties, ease of processability, and support for *in vitro* and *in vivo* tissue growth [23]. Composite scaffolds composed of PCL blended with BG-WS or BG-YS (80:20 wt%) were fabricated using melt-extrusion AM, characterized and evaluated *in vitro* for their osteogenic, angiogenic, as well as immunomodulatory properties using clinically relevant human mesenchymal stromal cells (hMSCs) and human umbilical vein endothelial cells (hUVECs).

2. Materials and methods

2.1. Raw materials

Medical grade PCL (PURASORB® PC08, $M_w = 51$ kDa) was provided by Corbion (Amsterdam, The Netherlands). All chemicals were bought from Merck KGaA (Darmstadt, Germany) unless stated otherwise.

BGs used in this study were previously synthesized and characterized [22] and their osteogenic as well as angiogenic properties were reported [18,19]. BGs were composed of silica sands and calcite extracted from natural resources. Depending on the depth of the deposit from which the sand was extracted, its corresponding colour varied: white sand (WS, quartzose sand, depth up to 0.7 m), and yellow sand (YS, quartzose sand, depth range 1.25 – 1.85 m). The content of potentially harmful elements present in both silica sands and calcite was below the limits established by the Standard Specification for Glass and Glass-Ceramics Biomaterials for Implantation (ASTM F1538), indicating that they could be used directly for biomedical use without the need for additional purification steps [22]. Starting from either WS or YS type of silica, corresponding glasses have been synthetized and termed BG-WS and BG-YS. The raw materials were combined with sodium carbonate anhydrous and subjected to a multi-step thermal treatment: the temperature was first increased to 650 °C at a rate of 2 K/min, then to 950 °C at 1 K/min, and finally to 1450 °C at 5K/min. The melt was maintained at 1450 °C for 3 h before being rapidly quenched onto stainless steel plates preheated to 400 °C. The resulting glasses were annealed at 450 °C for 2 h and then gradually cooled down [22]. The BG-WS and BG-YS powders were obtained as larger pellets (mm sized) and were treated with ball milling for 90 min to reduce the particle size to facilitate powder processability. To assess the obtained particle size, the powders were gold-coated (Cressington sputter coater 108 Auto) and imaged with scanning electron microscopy (SEM, Jeol JSM-IT200 InTouchScope, Tokyo, Japan), with a voltage of 10 kV and a working distance of 10 mm. Finally, the chemical composition of the powders was validated via an energy-dispersed X-ray spectroscopy (EDX) analysis.

SEM images were manually quantified using the software *ImageJ* to determine particle size. Three images per glass type were analyzed and for each of them 25 measurements were taken, including all particles with size in the biggest range and smaller particles through random selection. Particle size was also quantified with dynamic light scattering (DLS, Malvern Zetasizer Nano ZS, Malvern Insturments Ltd.). Measurements were conducted at room temperature, by suspending 0.1% w/v of particles in dH_2O. Sonication was applied prior measurement to promote particle homogenous suspension.

2.2. Preparation and characterization of PCL/BG composites

Starting from BG-WS and BG-YS powders, two composite materials

were produced, PCL/BG-WS or PCL/BG-YS, following a previously optimized blending method [24]. Briefly, BG-WS or BG-YS powders were added to PCL dissolved in tetrahydrofuran, in a PCL:BG ratio 80:20 w/w. A 20% w/v glass content was selected as the highest that allowed reliable and reproducible printing process, without clogging or loss of printing fidelity. Once the powders were homogeneously dispersed in the solution through mechanical stirring, the composites were precipitated in ethanol and dried in the vacuum oven at 30 °C overnight to remove excess of solvent [24]. The chemical composition of the composites was validated via X-Ray Diffraction (XRD, D2 phaser, Bruker, Massachusetts, USA) and Fourier-Transform Infrared Spectroscopy (FTIR, Nicolet iS50, Thermo Scientific, Massachusetts, USA). XRD analysis was performed in the range $7^\circ \leq 2\theta \leq 60^\circ$, and increments of 0.02°, while the FTIR was conducted in the 4000-400 cm^{-1} range, running 16 background scans and 32 scans. Raw BG powders and PCL were included in the analysis as controls.

Thermogravimetric analysis (TGA, TA Instruments TGA550) was conducted to quantify glass content in PCL/BG-WS and PCL/BG-YS composites. PCL only was used as control. Briefly, materials were heated to 500 °C with a temperature ramp of 10 °C·min^{-1}. Weight percentage was plotted as a function of temperature.

2.3. Scaffold fabrication and alkaline surface etching

PCL only and composite scaffolds, PCL/BG-WS and PCL/BG-YS, were printed with an in-house developed extrusion-based printer [25]. The materials were added to the reservoir and heated at T = 95 °C and T = 120 °C for PCL and composites, respectively. Then, the melted materials were extruded through a 22G nozzle, with a pressure of 3 bar, and a 7.5 rpm screw speed. The extruded filament was deposited at a 3 mm/s translational speed. A star-shaped pore geometry was generated with a GESIM Bioscaffolder software (Radeberg, Germany, version 3.0), setting a rotation of 15 degrees of consecutive printing layers. The geometry was selected based on a previous study, where its osteogenic and minerlization potential was assessed [24]. The geometry was designed by setting a strand distance and a layer thickness of 0.9 mm and 0.33 mm, respectively. Cylindrical scaffolds with 6 mm diameter and 4 mm height were printed for mechanical testing, while for cell culture and degradation experiments, 6 mm diameter and 2 mm height samples were fabricated. Subsequently, the scaffolds were pre-wetted in 70% v/v ethanol for 30 min and then treated for 2 h in a 5 M NaOH solution at 37 °C, to degrade the superficial layer of the polymer and expose the BG particles to the external environment.

2.4. Scaffolds characterization

2.4.1. Morphology

The printed scaffolds were gold-coated with a Cressington sputter coater 108 Auto and imaged with SEM, with a voltage of 10 kV and a working distance of 10 mm. Subsequently, the Fiji Software (version ImageJ2) was used to measure morphological parameters, such as fiber diameter, strand distance, layer thickness, and evaluate the printing fidelity. Moreover, the distribution of the BG particles within the fiber and the efficiency of the NaOH treatment were validated.

The porosity of the AM scaffolds was estimated, following a gravimetric method. Briefly, the total porosity was determined from the density of the bulk material and the scaffold, according to the following formula (1):

$$Total\ porosity\ [\%] = 1 - \frac{\rho_{scaffold}}{\rho_{material}} \quad (1)$$

Where: $\rho_{scaffold} = \frac{mass}{volume}$; $\rho_{material} \sim 1.145 - 1.456\ g/cm^3$.

2.4.2. Mechanical testing

Mechanical properties of the polymer and composite scaffolds were determined upon compression using a TA ElectroForce system (TA Instruments, Delaware, USA), a 450 N load cell, and controlled with Wint7 software. A 0.04 mm s^{-1} strain rate up to 50% compression was applied. Three replicates of PCL, PCL/BG-WS and PCL/BG-YS were tested. The stress-strain curves were derived by dividing the measured load against the net fiber area, calculated as described in previous research studies [24,26]. From the stress-strain curves, the compressive moduli of the constructs were calculated in a 5-15% strain range in the linear region.

2.4.3. Degradation, ion release and pH measurements

The degradation of the scaffolds was assessed using three samples of each type. In order to simulate physiological conditions, the samples were incubated in phosphate buffer saline (PBS) containing a physiological concentration of the enzyme lipase (Lip), namely 102 U/l [27,28]. Prior to the experiment, the scaffolds were weighted and subsequently placed in a 24-well plate containing 2 ml of either PBS or PBS supplemented with lipase (PBS + Lip). The samples were incubated at 37 °C for 28 days, with the buffer being replaced every 2-3 days, and the medium was stored for further analysis. At different time points the scaffolds were collected, dried on absorbent paper from the excess of buffer and weighted. The weight loss percentage was calculated according to formula (2):

$$Weight\ loss\ [\%] = \left|\frac{Wf - Wi}{Wi}\right| \times 100 \quad (2)$$

Where:

Wi = initial weight.

Wf = final weight.

The buffer collected at each degradation time point was analyzed to measure the concentration of biologically relevant ions, Si^{4+}, Ca^{2+}, Ti^{4+}, Fe^{3+}, and Al^{3+}. The cumulative release of these ions was quantified by inductively coupled plasma mass spectrometry (ICP-MS, iCAP Q, Thermo Scientific, Massachusetts, USA) in standard mode. Samples were diluted 20 times in 1% v/v nitric acid solution containing 20 ppb scandium as internal standard. For quantification, standard curves in the range of 0.3 - 4.8 ppm for Ca^{2+} and Si^{2+} and 0.001 – 0.01 ppm for Ti^{4+} and Fe^{3+} were used. Al^{3+} ions were not possible to quantify due to the very low concentration and low quality of the measurements. To assess the potential effect of ion release on pH changes, scaffolds were immersed in basic cell culture medium and placed in a cell culture incubator (5% CO_2, 37 °C). The medium was collected daily and its pH measured, until stabilization around physiological values.

2.5. In vitro studies

After washing the scaffolds in water, they were disinfected by immersion in 70% ethanol for 30 min, followed by washing steps. Finally, scaffolds were incubated in a basic culture medium composed of α-MEM (Thermo Fisher, Landsmeer, The Netherlands) supplemented with 10% Fetal bovine serum (VWR, Amsterdam, The Netherlands), and 0.2 mM ascorbic acid at 37 °C, 5% CO_2 for 3 days, changing the medium every 24 h to neutralize the pH.

2.6. Direct 3D cell culture

hMSCs used in this study were isolated from bone marrow aspirates obtained from one donor, who has given written consent. The studies involving human participants were reviewed and approved by the Medical Ethical Committee (METC) of the Maastricht University Medical Center (#15–4-274). hMSCs were cultured in a basic culture medium at 37 °C under 5% CO_2. The culture medium was changed 24 h after seeding and twice a week during expansion. Prior to cell seeding, the scaffolds were incubated in basic culture medium overnight to allow protein adsorption. After that, the medium was discarded, and scaffolds were dried on blotting paper and placed into 24 well plates. hMSCs at

passage 5 were seeded at a density of 200 000 cells per scaffold in a basic culture medium containing 10% of Dextran (Pharmacosmos, Holbæk, Denmark). Cell-seeded scaffolds were incubated for 4 h to facilitate cell attachment, after which 1.5 mL of basic medium was added. Culture on 3D scaffolds was performed in the above-mentioned basic growth medium with the addition of 100 U/mL penicillin +100 mg/mL streptomycin (Thermo Fisher, Landsmeer, The Netherlands) and, in the case of positive osteogenic control, with the addition of 10 nM Dexamethasone. Medium was refreshed every 24 h for the first 3 days of culture and every 2-3 days afterwards. Cell culture supernatant was collected on days 3, 7, and 28 for downstream analysis.

2.7. Osteogenic gene expression

Total RNA was isolated from hMSCs cultured on composite scaffolds for 7 and 28 days using TRIZOL (Thermo Fisher, Landsmeer, The Netherlands), chloroform, and isopropanol. The selected time points were chosen to capture both early and late stages of osteogenic differentiation, with day 7 reflecting early osteogenic commitment and day 28 representing matrix maturation and mineralization. The RNA concentration was measured using a Bio-drop μLITE instrument (Harvard Biosciences, Massachusetts, USA). cDNA was synthesized using an iScript cDNA synthesis kit (Bio-Rad, California, USA) according to the manufacturer's protocol and diluted in RNAse-free water 10 times. The qPCR measurement was performed with Bio-Rad Thermal Cycler (CFX96 Touch Real-Time PCR Detection System, Bio-Rad, California, USA) using Sybr green master mix (Bio-Rad, California, USA). The sequences of the used primers are listed in Table 1. Gene expression of *RUNX2*, *ALPL*, *COL1A1*, and *BGLAP* (also known as *OCN* for simplification), was normalized to the housekeeping gene *YWHAZ,* and fold gene expression was calculated using the ΔΔ Ct method. Regarding *OCN* expression, due to low and in some cases undetectable expression at day 7, not all replicates yielded quantifiable CT values. Consequently, the number of data points included in the 2^(−ΔΔCt) calculations were reduced (n = 2 for PCL/BG-YS in basic medium, n = 1 for PCL/BG-WS in osteogenic medium, and n = 2 for PCL/BG-YS in osteogenic medium).

2.8. DNA content, ALP activity and collagen quantification

Cell Proliferation Assay Kit CyQUANT® (Thermo Fisher, Landsmeer, The Netherlands) was used following the manufacturer's instructions to measure the total DNA content per scaffold on days 7, and 28 of culture. Samples were washed three times with PBS and stored overnight at −80 °C. Thereafter, samples were freeze-thawed three times. Lysis buffer composed of 0.1 M KH_2PO_4, 0.1 M K_2HPO_4, and 0.1% Triton X-100 (pH 7.8) was added to each sample and incubated for 1 h at room temperature. To assess the ALP activity, 10 μL of the lysed sample was added in triplicates to a white 96-well plate. Next, 40 μL of a CDP-star reagent (Roche Applied Science, Penzberg, Germany) was added to the samples and incubated for 15 min in the dark. Absorbance was measured at 466 nm. Obtained values were normalized to the DNA content. The remaining samples were treated with 1 mg/ml proteinase K (Merck, Darmstadt, Germany) solution and incubated overnight at 52 °C while shaking. Samples were then freeze-thawed three times and a lysis buffer containing RNase A (Thermo Fisher, Landsmeer, The Netherlands) was added in a ratio of 1:1 to each sample. Finally, 100 μL of the digested sample was added to a black 96 well plate followed by further addition of 100 μL of the GR-dye solution. After 15 min of incubation, fluorescence was measured at emission wavelength 520 nm and excitation wavelength 480 nm. To measure the total collagen content in the samples, a Collagen Assay Kit (Merck Darmstadt, Germany) was used. The proteinase K digested samples were used for this purpose and the obtained results were normalized to the DNA content. The assay reaction mix was prepared by mixing the provided buffer and digest enzyme and added to the samples in a 96-well plate following the manufacturer's instructions. After 60 min of incubation at 37 °C, a dye reagent was added and further incubated for 10 min at 37 °C. After that, a developer solution was added to all wells and further incubated for 10 min at 37 °C. Finally, fluorescence was read at an excitation of 375 nm and an emission of 465 nm.

Table 1
Primer sequences of the analyzed genes.

GENE	SEQUENCES
YWHAZ **(Tyrosine 3-monooxygenase/tryptophan 5-monooxygenase activation protein zeta)**	**F**: CCTGCATGAAGTCTGTAACTGAG **R**: GACCTACGGGCTCCTACAACA
RUNX2 **(Runt-related transcription factor 2)**	**F**: TCAACGATCTGAGATTTGTGGG **R**: GGGGAGGATTTGTGAAGACGG
ALPL **(Alkaline Phosphatase)**	**F**: ACAAGCACTCCCACTTCATC **R**: TTCAGCTCGTACTGCATGTC
COL1A1 **(Collagen type I alpha 1 chain)**	**F**: CGGTGGTTTCTTGGTCGGT **R**: GTGCGATGACGTGATCTGTGA
BGLAP also known as OCN **(Osteocalcin)**	**F**: TGAGAGCCCTCACACTCCTC **R**: CGCCTGGGTCTCTTCACTAC
VEGFA **(vascular endothelial growth factor A)**	**F**: ATCTTCAAGCCATCCTGTGTGC **R**: GCTCACCGCCTCGGCTTGT

2.9. Tubule formation assay

Human umbilical vein endothelial cells (HUVECs) (Lonza, Basel, Switzerland) were cultured in an endothelial growth medium (EGM, Lonza, Basel, Switzerland) without VEGF supplementation at 37 °C and 5% CO_2. A tubule formation assay was performed in a 96 well μ-Plate (ibidi, Gräfelfing, Germany). Wells were coated with 10 μL of Geltrex™ (Thermo Fisher Landsmeer, The Netherlands) per well, according to the manufacturer's instructions. HUVECs at passage 3 were incubated with Calcein-AM (Thermo Fisher Landsmeer, The Netherlands) for 20 min prior seeding at a density of 40 000 cells/cm^2 in EGM, serving as a control, with EGM + 200 ng/mL VEGF peptide (Miltenyi Biotec, Bergisch Gladbach, Germany) serving as positive control, and EGM + αMEM collected from the culture of hMSCs on each scaffold for 7 and 28 days (at a ratio 75:25) serving as the experimental condition. After 6 h of incubation, cells were imaged using an automated inverted Nikon Ti-E microscope (Nikon Instruments Europe BV, Amsterdam, The Netherlands), equipped with a Lumencor Spectra light source (Oregon, USA), an Andor Zyla 5.5 sCMOS camera (Oxford Instruments, Abingdon, United Kingdom), and an MCL NANO Z200-N TI z-stage (Mad City Labs GmbH, Zurich, Switzerland). Tubular parameters were quantified using Fiji software with Angiogenesis analyser Plug-in (U.S. National Institutes of Health, USA).

2.10. Detection of specific cytokines using a multiplex assay

Human ProcartaPlex 10-plex (Invitrogen, Amsterdam, The Netherlands) multiplex assay was used to measure concentrations of several anti-, pro-inflammatory as well as pro-angiogenic cytokines and

Table 2
List of analytes measured with ProcartaPlex 10-plex multiplex assay and their abbreviations.

ABBREVIATION	FULL NAME
IDO	Indoleamine 2,3-Dioxygenase
IL-10	Interleukin 10
INF-γ	Interferon-gamma
TNF-α	Tumour necrosis factor-alpha
CCL5	C–C motif chemokine ligand 5
IL-6	Interleukin 6
IL-1β	Interleukin 1 beta
CCL2	C–C motif chemokine ligand 2
MMP-8	Matrix metalloproteinase-8 collagenase
VEGF-A	Vascular endothelial growth factor A

chemokines in the supernatant of direct culture of hMSCs on different 3D composite scaffolds. A list of the analyzed cytokines is presented in Table 2. Supernatants were collected on days 7 and 28. At each time point, samples (n = 3) were used to measure the average concentrations in duplicates. Samples were diluted 2x in the provided universal assay buffer (based on preliminary experiments). The assay was performed following the manufacturer's instructions. Briefly, capture beads were added to the supplied 96-well plate. The wells were washed twice using a magnet to secure the beads in the wells. Then, samples and antigen standards were added, and the plate was sealed, shaken for 30 min at room temperature, then transferred to 4°C and stored on a level surface. After an overnight incubation, the plate was shaken for an additional 30 min at room temperature. The washing step was repeated twice. Next, a provided mix of antibodies was added into each well and the plate was sealed and incubated for 30 min. Then, the plate was washed twice, and Streptavidin-PE was added for another 30 min while shaking. The plate was washed twice, and the beads were resuspended in a reading buffer. The data was acquired using the Luminex 200 xPONENT 3.1 instrument (Invitrogen, Amsterdam, The Netherlands). Data was analyzed using the ProcartaPlex Analysis App, a software available through the Connect cloud-based platform of Thermo Fisher Scientific (Landsmeer, The Netherlands). The results are reported as raw data as well as normalized to the DNA content measured with CyQUANT DNA assay.

2.11. Statistical analysis

All the results are expressed as means ± standard deviation. All experiments were performed once in biological triplicates. The statistical analysis was performed with GraphPad Prism 10 (GraphPad software, California, USA). After assessment of the normality of data distribution with the Shapiro-Wilk test, the statistical significance was determined with parametric ANOVA with Tukey's multiple comparison test. Otherwise, non-parametric tests were performed. qPCR results were analyzed with ordinary one-way ANOVA followed by Dunnett's multiple comparison test. Tubule formation assay quantification results, DNA and ALP activity quantification, as well as multiplex data were analyzed with two-way ANOVA followed by Tukey's multiple comparison test. Levels of statistical significance are indicated by * $p < 0.05$, ** $p < 0.01$, *** $p < 0.001$ and **** $p < 0.0001$.

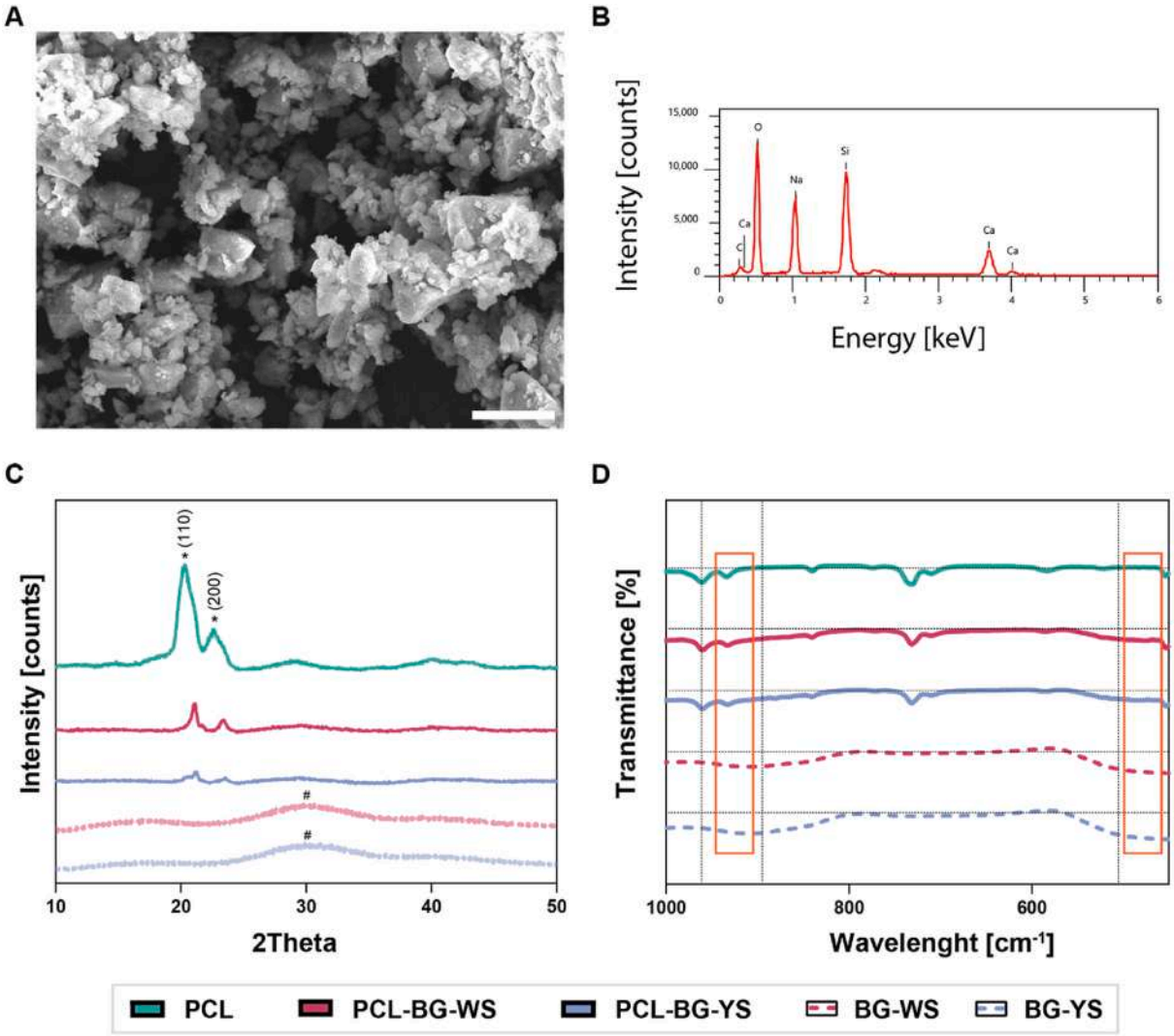

Fig. 1. Representative SEM image of BG-WS powder after ball milling. Scale bar = 5 μm (**A**). EDX analysis of BG-WS powder showing the presence of Si, Na and Ca as main elements (**B**). XRD of PCL, powders and composites. PCL peaks are visible at 2θ values of 20.3° (110) and 22.6° (200), amorphous silica peak shown at 2θ = 30.1° (**C**). Zoom of the FTIR spectra between 1000 and 400 cm^{-1} of PCL, powders and composites, displaying Si–O–Si stretching (897 cm^{-1}) and bending (492 cm^{-1}) (**D**). Data represents n = 3 biological replicates from one independent experiment.

3. Results and discussion

3.1. Composite preparation and characterization

After ball milling treatment, the glass particles were assessed using SEM imaging, showing a qualitative final size range of 1–10 μm (Fig. 1A and Fig. S1A). Quantification of the SEM images resulted in an average particle size of 2.55 ± 2.18 μm for BG-WS and 2.17 ± 1.79 μm for BG-YS powders (Fig. S1C). In contrast, DLS measurements indicated a smaller particle size range, with values of approximately 1 μm (Fig. S1D–E). This difference is likely attributed to an underestimation of particle size occurring during DLS measurement due to particle sedimentation, which was observed by the authors despite the initial sonication step. For this reason, particle size estimation obtained from SEM images was considered more reliable.

The EDX analysis displayed peaks for Si, Ca, and Na (Fig. 1B), confirming that the glasses mainly consist of SiO_2, Na_2O, and CaO. The spectrum did not show peaks corresponding to P ions, confirming the absence of detectable amounts of P_2O_5 in the BGs composition.

Subsequently, composites of PCL/BG-WS and PCL/BG-YS were produced according to a blending method [24], incorporating 20% (w/w) of BG, and their final chemical composition was characterized via XRD and FT-IR. The XRD diffraction pattern (Fig. 1C) revealed the presence in the composites of the two PCL peaks, at 2θ values of 20.3° and 22.6°,

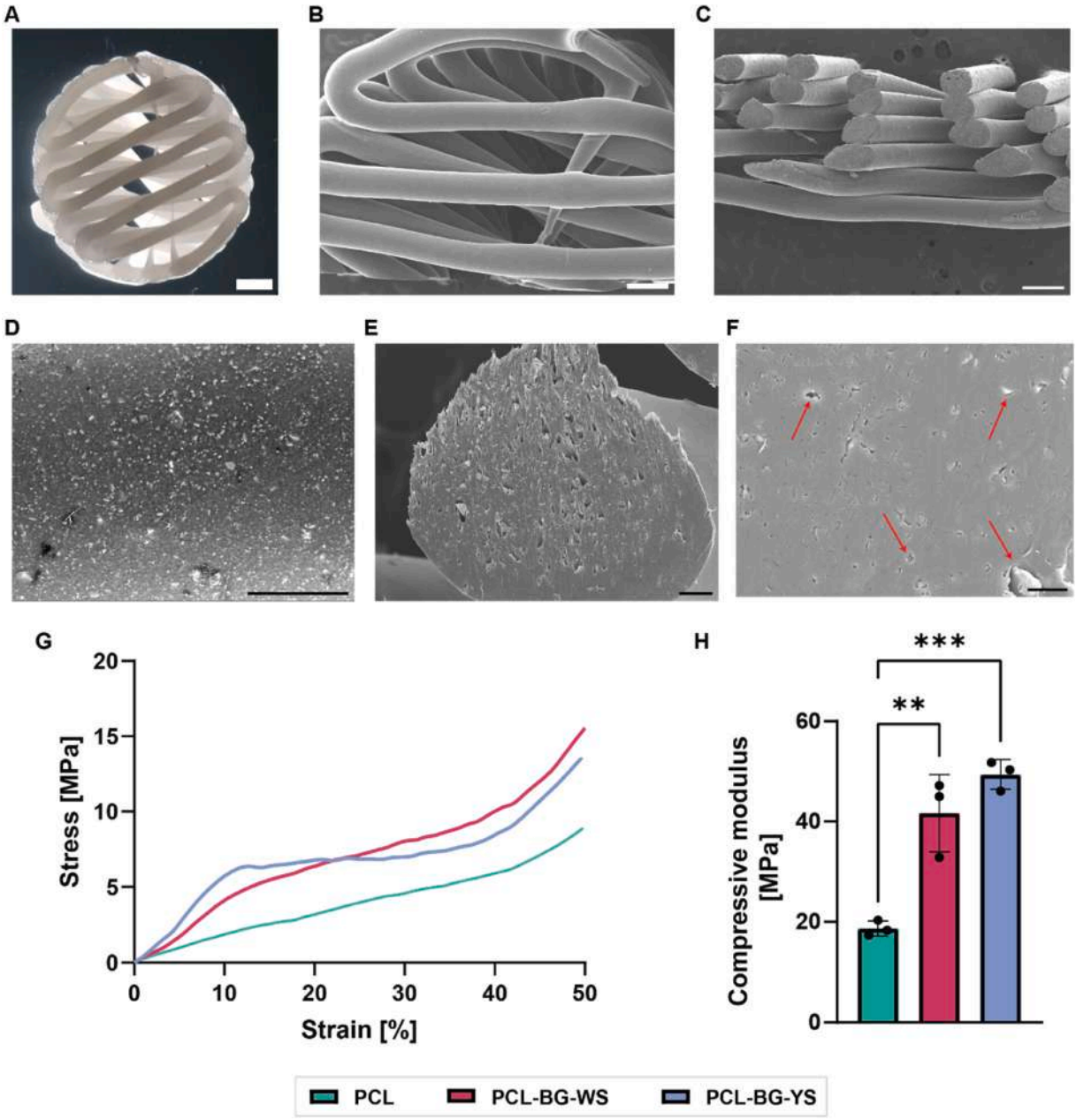

Fig. 2. Representative stereomicroscope image of a PCL scaffold with star-shaped pores. Scale bar = 1000 μm (**A**). Representative SEM image of PCL/BG-WS composite scaffold. Scale bar = 500 μm. Top view (**B**) and cross section (**C**). SEM image of PCL/BG-WS fiber surface, displaying homogenous particle distribution. Scale bar = 50 μm (**D**). SEM image of PCL/BG-WS fiber cross section, showing a uniform particle distribution. Scale bar = 50 μm (**E**). Zoom on the PCL/BG-WS fiber surface after NaOH treatment, showing the presence of cracks (indicated by the red arrows) on the surface of the fibers. Scale bar = 5 μm (**F**). Stress-strain curves of PCL, PCL/BG-WS and PCL/BG-YS scaffolds (**G**). Compressive moduli of PCL, PCL/BG-WS and PCL/BG-YS scaffolds (**H**). Levels of statistical significance represented by **p < 0.01, ***p < 0.001. Data represents n = 3 biological replicates from one independent experiment. (For interpretation of the references to colour in this figure legend, the reader is referred to the Web version of this article.)

corresponding to the (110) and (200) crystallographic planes, respectively [29], and the broad peak of the amorphous silica, at $2\theta = 30.1°$ [19,22]. The FT-IR analysis confirmed both the presence of PCL and BG groups in the composite materials. The stretching vibrations of CH_2 were identified at 2943 cm^{-1} and 2862 cm^{-1}, and the C═O stretching was detected at 1725 cm^{-1} (Fig. S1B) [29]. Additionally, the BG powders contributed to a broad deflection in the baseline of the transmittance curve around 897 cm^{-1} and 492 cm^{-1} (Fig. 1D), corresponding to the Si–O–Si symmetric stretching and to the Si–O–Si bending, respectively [30]. TGA measurements displayed a glass content of approximately 25% in both PCL/BG-WS and PCL/BG-YS composites, implying high efficiency of the blending strategy used to obtain the materials (Fig. S1F).

3.2. Scaffold fabrication and characterization

Porous PCL, PCL/BG-WS and PCL-BG/YS scaffolds were successfully fabricated with an in-house developed extrusion-based printer (Fig. S2A). The constructs were designed to have a star shape pore geometry as shown in the microscopy images and the CAD model view (Fig. 2A–C and Figure S2B-D, G). This particular pore shape was selected based on evidence that the cells commit towards an osteogenic phenotype when cultured on acute-angled pores, more than on the traditional woodpile structure [31]. Moreover, the star-shaped pore geometry was previously characterized and demonstrated pore interconnectivity and high reproducibility [24]. The morphological features such as fiber diameter, strand-strand distance, and layer thickness displayed values comparable to the theoretical ones of the model, indicating a good printing fidelity (Fig. S2L). A total porosity of around 53.7 ± 5.7% was estimated fot the AM scaffolds. The BG particles were homogenously distributed in the scaffold fibers (Fig. 2D and Fig. S2E) and in their cross-section (Fig. 2E).

Notably, previous studies reported that inorganic particles were covered by a thin polymer layer when produced with AM, leading to reduced/delayed biological effects [19,32]. Therefore, all scaffolds were subjected to a surface treatment with 5 M NaOH. The formation of cracks on the scaffolds' surface was observed and the BG particles were exposed, confirming the success of the etching treatment (Fig. 2F, Fig. S2F).

Subsequently, the mechanical properties of the NaOH-treated scaffolds was evaluated upon compression. A behaviour typical for scaffolds was observed, comprising an initial elastic region, followed by a plastic deformation phase. A second increase in the modulus was recorded at a higher strain, as a result of the closure of the pores (Fig. 2G). Both PCL/BG-WS and PCL/BG-YS scaffolds displayed, in the linear region of the stress-strain curves, higher compressive moduli compared to the PCL only ones, reaching values of 41.66 ± 7.73 MPa and 49.40 ± 2.95 MPa, respectively (Fig. 2H). This was likely a result of the presence of 20% w/w of bioactive glasses powders in the composites, which reinforced the PCL matrix. Similar behaviour was observed in other studies where the addition of 10% w/w or 20% w/w of bioactive glass particles to a PCL matrix induced a significant increase of the compressive moduli [19,33].

3.3. Scaffold degradation and ion release

After scaffold fabrication and characterization, the degradation of PCL, PCL/BG-WS, and PCL/BG-YS samples after NaOH treatment was investigated in a physiological-like environment, by supplementing PBS

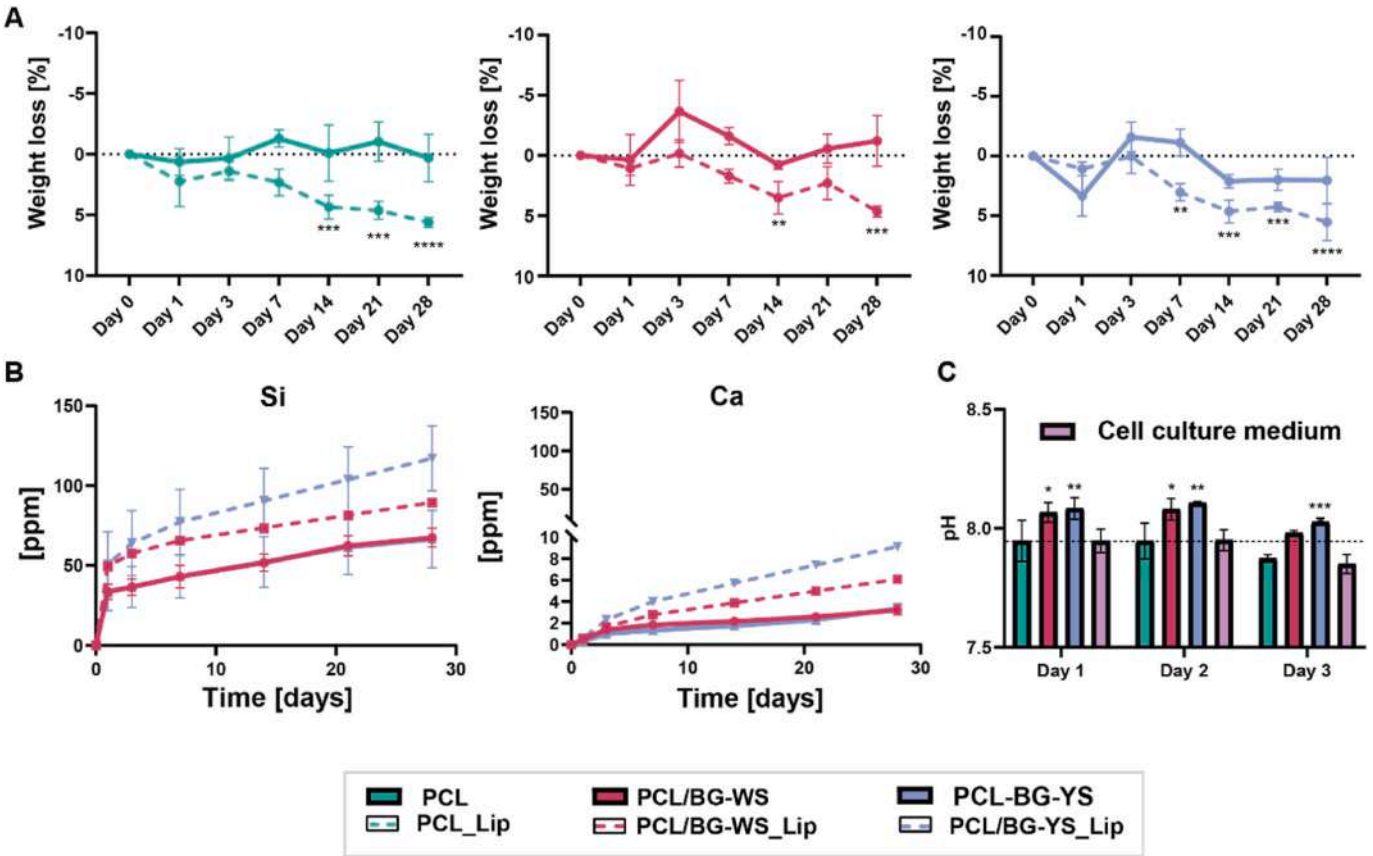

Fig. 3. Degradation in PBS or PBS + Lipase of PCL, PCL/BG-WS and PCL/BG-YS scaffolds for 28 days (**A**). Cumulative release of Si^{4+} and Ca^{2+} ions from PCL/BG-WS and PCL/BG-YS scaffolds in PBS and PBS + Lipase for 28 days (**B**). pH variation of basic culture medium incubated with PCL, PCL/BG-WS and PCL/BG-YS scaffolds over 3 days, without enzyme (**C**). Values were compared to the cell culture medium. Levels of statistical significance represented by * $p < 0.05$, ** $p < 0.01$, *** $p < 0.001$ and **** $p < 0.0001$. Data represents $n = 3$ biological replicates from one independent experiment.

with lipase. This enzyme is able to degrade PCL scaffolds [27]. Therefore, the weight loss percentage of the scaffolds over time was calculated, up to 28 days of incubation (Fig. 3A). All the scaffolds showed an approximately constant weight when incubated in only PBS. However, in PBS supplemented with the enzyme, PCL/BG-YS scaffolds displayed a significant weight loss after 7 days and PCL/BG-WS after 14 days. At 28 days all the samples reached a total weight loss percentage of 5.61 ± 0.41 %, 4.64 ± 0.45 %, and 5.54 ± 1.52 % for PCL, PCL/BG-WS and PCL/BG-YS, respectively. The presence of the enzyme contributed to the accelerated degradation, as previously reported in the literature. For instance, Martins et al. showed degradation of PCL scaffolds around 5-7% after 30 days of immersion in PBS containing 110 U/L of lipase [27]. Duarte et al. incubated PCL scaffolds in PBS with lipase 102 U/l for 21 days while shaking, recording a weight loss percentage between 10 and 20% [34].

In parallel to the scaffold degradation, the cumulative release of two biologically relevant ions, Si^{4+} and Ca^{2+}, from PCL/BG-WS and PCL/BG-YS scaffolds was recorded over 28 days of degradation. The release of Si^{4+} and Ca^{2+} ions from bioactive glasses plays a crucial role in osteogenesis and angiogenesis. A literature review reported several studies showing that the synergistic effect of these ions induced an increase in metabolic activity, ALP activity and VEGF production [35]. In both PBS only and PBS containing lipase, an increasing concentration of Si^{4+} and Ca^{2+} ions was observed, with higher values in the presence of the enzyme. The release of Si^{4+} reached the highest concentration of 117.0 ± 20.43 ppm, for PCL/BG-YS scaffolds in PBS with lipase, with a burst release of 50.66 ± 20.43 ppm in the first 24h (Fig. S3A). The amount of Ca^{2+} ions reached a much lower cumulative release of 9.13 ± 0.07 ppm, and no initial burst release (Fig. S3A). The higher ion release observed for the PCL/BG-YS composites in the presence of lipase may be attributed to the inhomogeneous and variable nature of the enzymatic degradation of the PCL matrix, which might have resulted in a different exposure of the embedded BG particles between the two composites.

In addition, trace levels of Ti^{4+} and Fe^{3+} ions were detected (Fig. S4). The cumulative release of these elements did not exceed 0.1 ppm for Ti^{4+} ions and 0.14 ppm in the case of Fe^{3+} ions. This low release was expected, as both elements are present in the BGs only at trace concentrations. Nevertheless, the release of these ions could still be detected, indicating measurable ion exchange between the composites and the surrounding fluid. Notably, these ions are known to exert biological effects even at very low concentrations [36,37].

Typically, the release of ions from the BGs leads to an increase in pH of the culture medium. Already a slightly basic pH of the medium has been shown to result in cell death during cell culture [19,38]. Therefore, prior to cell seeding, PCL, PCL/BG-WS, and PCL/BG-YS were incubated in cell culture medium for 3 days, measuring the pH every day. In the first 48h of incubation, a significant increase in the pH values in the media incubated with composite scaffolds was measured (Fig. 3C), implying even higher local pH values directly at the scaffold interface where the ions are released than what reported by Brauer [38]. The pH variation was also qualitatively confirmed by a change of colour of the medium, which turned bright pink after 24h (Fig. S3B). On the third day, a stabilization of the pH values around 7.8 was observed. The results suggested that, prior to cell seeding, the scaffolds should be incubated in media for 3 days to maintain a physiological pH during cell culture and prevent cell death. A similar strategy was also followed by other groups, who performed pre-incubation of 3 to 7 days prior cell seeding, to bring pH values from above 8 in the first hours to physiological levels [39,40]. This suggests that the initial alkalinization associated with BG dissolution is transient and can be effectively mitigated through pre-incubation, allowing the beneficial ionic effects of the composite scaffolds to be studied without confounding cytotoxicity.

3.4. Angiogenic properties

Angiogenic properties of the scaffolds were assessed by analysing the *VEGFA* gene expression (Fig. 4A) of hMSCs cultured directly on scaffolds for 7 and 28 days, quantification of the VEGFA secreted into the cell culture medium (Fig. 4B), as well as through an assessment of tubule-like structure formation of HUVECs cultured in medium conditioned by the scaffolds for 7 or 28 days (Fig. 4C).

While at day 7 the gene expression of *VEGFA* was comparable among conditions, at day 28 its expression was upregulated on PCL/BG-WS composites compared to PCL scaffolds (fold change value of 1.43 ± 0.17). Interestingly, on the protein level, VEGFA concentrations were significantly higher at day 7 than at day 28 on all investigated scaffolds (Fig. 4B), which suggests that the upregulation of the gene expression might have occurred at an earlier time point than investigated in this study. Furthermore, at both time points the concentrations of VEGFA were significantly higher on PCL/BG-WS and PCL/BG-YS scaffolds when compared to scaffolds comprising PCL alone. Additionally, tubule-like structure formation by HUVECs exposed to a conditioned medium containing dissolution products of each investigated scaffold and the corresponding quantification of the tubular parameters are shown in Fig. 4C. HUVECs, as well as other endothelial cells, will grow on a soft substrate and form tubular networks ranging from short and isolated segments to highly developed meshing, depending on the treatment conditions [41]. Greater network complexity, reflected by increased junction number, total length, and mesh size, is generally interpreted as enhanced angiogenic potential. Therefore, this is a very commonly used *in vitro* angiogenesis assay used to identify inhibitors or stimulators of angiogenesis [42]. In this study, tubular structures formed in each condition with a slightly higher number of junctions and total length quantified in the case of cells exposed to medium collected at day 7 than at day 28 for PCL/BG-WS. Mean mesh size, however, was significantly higher for cells exposed to medium collected at day 28 compared to day 7 for PCL/BG-YS scaffolds. Additionally, at day 28 both composite scaffolds (PCL/BG-WS and PCL/BG-YS) exhibited significantly greater mean mesh sizes (8136.5 ± 2376.9 μm^2 and 8103.0 ± 1548.6 μm^2, respectively) compared to PCL alone. No statistically significant differences were observed compared to the EGM and EGM + VEGF controls (Fig. S5).

The observed enhanced angiogenic effect in both composite scaffolds may be attributed to the presence of BGs, as it has been previously reported that silicate-based glasses have been linked with induction of angiogenic differentiation and upregulation of genes related to angiogenesis [14,15]. BG dissolution products, in particular Si^{4+} ions, have been shown to promote angiogenic signaling and endothelial cell organization [43]. Additionally, the distinct trace element profiles of the two BGs, higher Ti^{4+} ions content in BG-WS and higher levels of Fe^{3+} and Al^{3+} in BG-YS might have contributed synergistically to the observed angiogenic effects [14,18,44]. However, the cumulative release of Ti^{4+} and Fe^{3+} from both PCL/BG-WS and PCL/BG-YS composite scaffolds was comparable and remained within the trace element range. Low concentrations were anticipated, since these elements are present in the BGs only as minor elements and the release measurements were performed on composites containing 20 wt% BG within the PCL matrix.

Previous studies investigating the angiogenic properties of polymer-BG composites including both benchmark 45S5 and commercially available S53P4 formulations, have consistently reported *VEGFA* gene upregulation across a range of BG chemistries, although the timing and magnitude of this response vary considerably depending on the BG composition, polymer matrix, and biological model employed. For example, PCL/BG composites including those based on SiO_2–Na_2O–CaO BGs [19] or custom Boron-containing BGs (B-BGs) [10] were shown to induce *VEGFA* gene upregulation at earlier culture time points than those investigated in our study, as reported for adipose-derived hMSCs and rat MSCs, respectively. With respect to polymer-BG composites

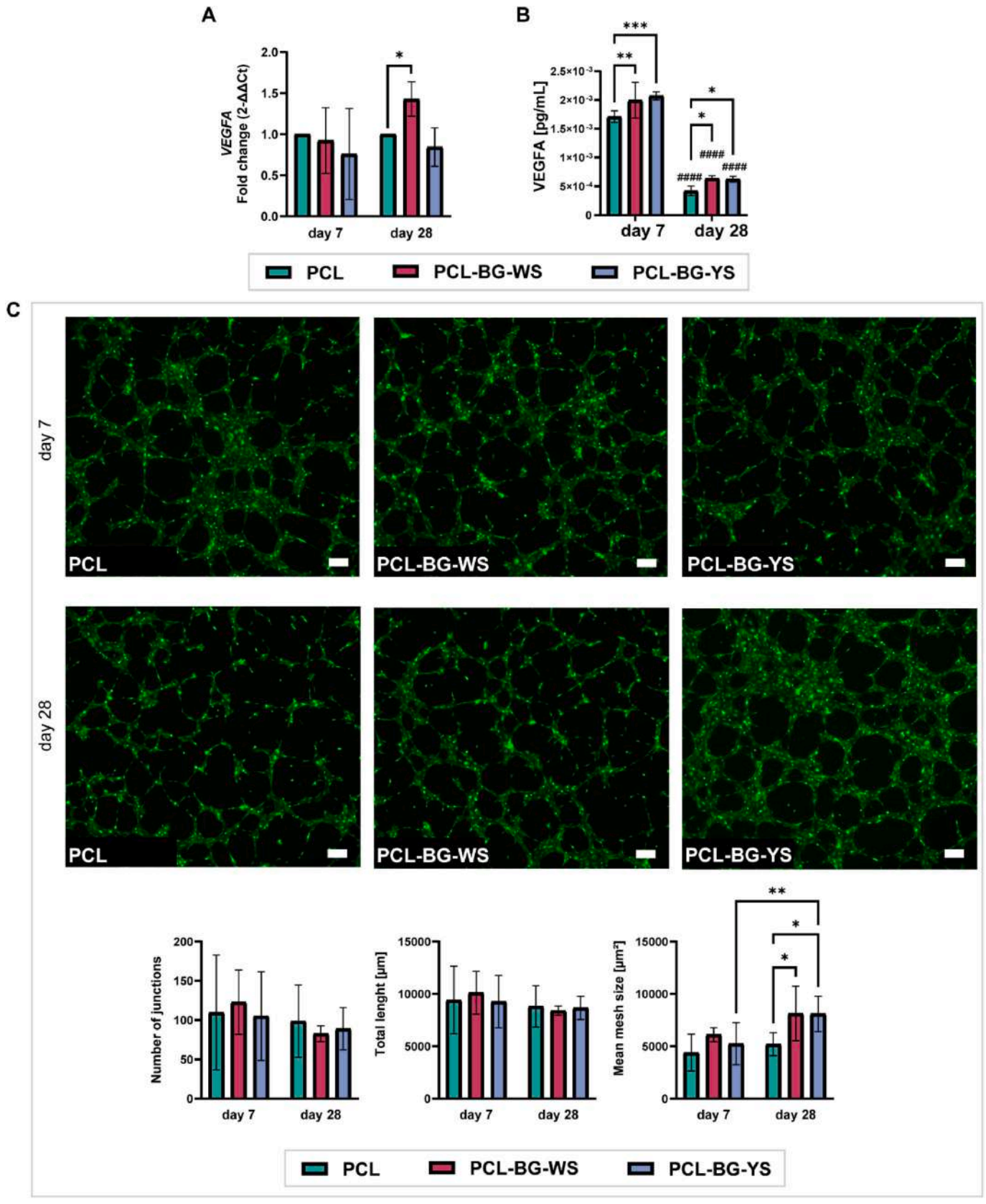

Fig. 4. Angiogenic properties of 3D scaffolds. **(A)** Expression of *VEGFA* by hMSCs cultured directly on 3D scaffolds for 7 and 28 days. **(B)** The concentration of VEGFA measured in the culture medium after 7 and 28 days of culture. **(C)** Tubule-like structure formation of HUVECs cultured with medium collected from a direct culture of hMSCs on 3D scaffolds for 7 days or 28 days and quantification of selected tubular parameters: number of junctions, total length, and mean mesh size. Scale bar = 200 µm. Green, fluorescent staining corresponds to Calcein-AM. Levels of statistical significance are indicated by * $p \leq 0.05$, ** $p \leq 0.01$, *** $p \leq 0.001$ and **** $p \leq 0.0001$. Data represents n = 3 biological replicates from one independent experiment. (For interpretation of the references to colour in this figure legend, the reader is referred to the Web version of this article.)

incorporating the benchmark 45S5-BG, Distler et al. [45] reported increased *VEGFA* gene expression in human adipose derived stem cells cultured on PLA scaffolds containing 45S5-BG after prolonged culture (35 days), indicating the delayed transcriptional responses can occur depending on the polymer-BG system and culture conditions. Similarly, Wu et al. [46] demonstrated enhanced *VEGFA* gene expression in co-cultures of hMSCs and HUVECs on Poly (3-hydroxybutyrate-co-3-hydroxyvalerate) (PHBV) scaffolds containing 45S5-BG at day 14, indicating early paracrine anagiogenic response driven by hMSCS-endothelial cells cross-talk. In comparison, the later *VEGFA* gene upregulation observed in the present study may reflect differences in culture system, polymer matrix, and the temporal dynamics of BG-derived ion signaling. Beyond the benchmark 45S5 Bioglass, S53P4-BG is another extensively studied and commercially available BG that has demonstrated angiogenic activity when incorporated into polymeric into constructs. For example, PLGA-coated S53P4 scaffolds were shown to increased *VEGFA* expression in the rabit induced-membrane model [47], highlighting the angiogenic relevance of S53P4-based composites *in vivo*.

Regarding angiogenic outcomes at the protein level, Gerhardt and colleagues [48] as well as Day et al. [49] independently demonstrated that incorporation of 45S5-BG into polymer matrices (PDLLA and PLGA, respectively) significantly enhances VEGFA secretion by fibroblasts in a filler content dependent manner, and that this increased release translates into improved vascularization *in vivo*. This finding further highlights the angiogenic potential of phosphorous-containing BGs when embedded into a polymer matrix and is consistent with the elevated VEGFA concentrations observed for the composite scaffolds in the present study. Similarly, a prolonged increase in VEGF secretion was reported for myofibroblasts cultured on PLGA microporous spheres incorporating 45S5 Bioglass [50], further supporting the ability of polymer-BG composites to sustain angiogenic signaling at protein level.

In addition to VEGFA expression and secretion, several studies have demonstrated enhanced endothelial tubule formation in response to dissolution products from PCL-based BG composites. For instance, Cichos et al. [51] demonstrated a concentration dependent increase in HUVEC junctions, segments, and total tubule length when exposed to conditioned medium from PLA/S53P4 composites, which is in line with the enhanced tubulogenesis observed in the present study. Similarly, Wang et al. [9] reported enhanced endothelial network formation in a

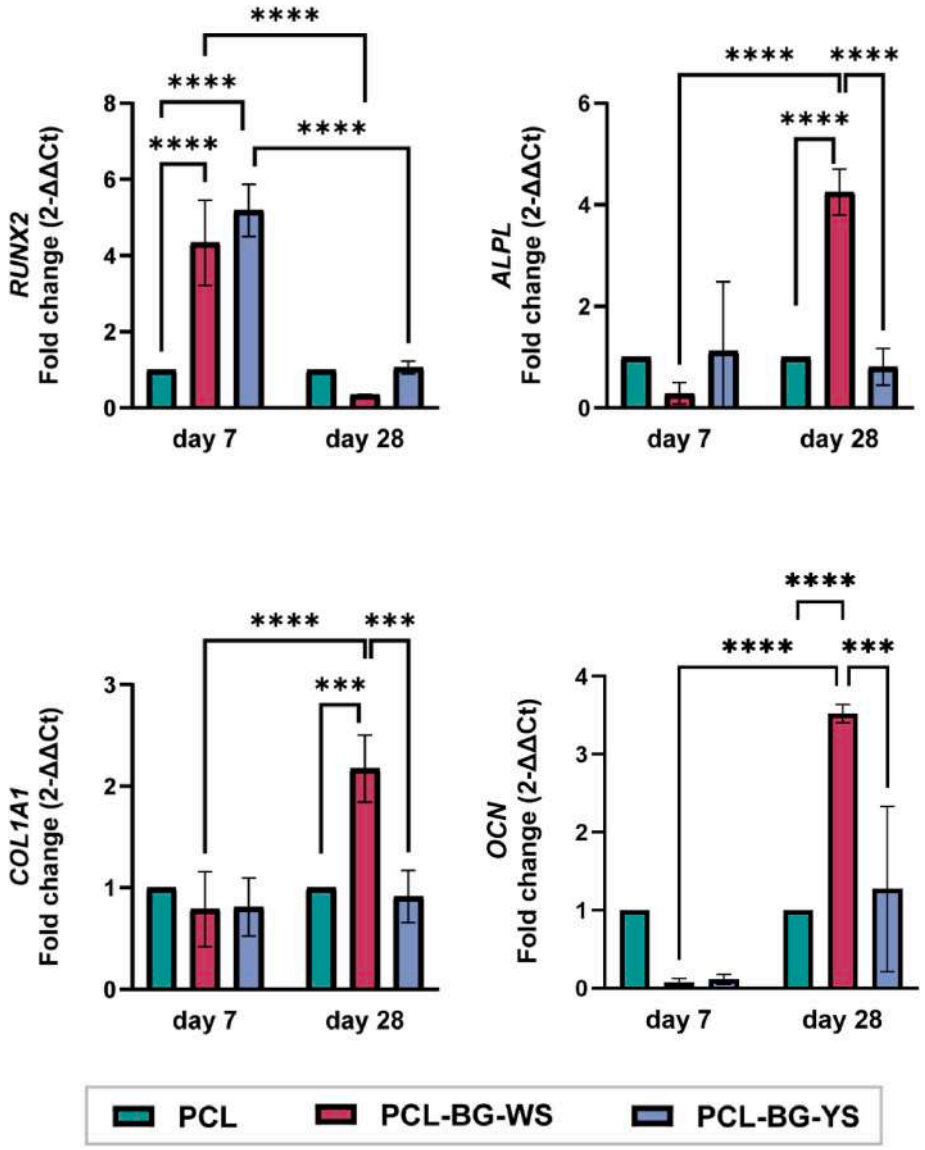

Fig. 5. Expression of *RUNX2*, *ALPL*, *COL1A1*, and *OCN* by hMSCs cultured on PCL, PCL-BG-WS, and PCL-BG-YS scaffolds for 7 and 28 days in basic culture medium. Results are shown as fold gene expression, normalized to the expression on the PCL sample using the ΔΔCT method. Levels of statistical significance are indicated by * $p \leq 0.05$, ** $p \leq 0.01$, *** $p \leq 0.001$ and **** $p \leq 0.0001$. Data represents $n = 3$ biological replicates from one independent experiment.

coculture of hMSCs and HUVECs on PCL scaffolds incorporating S53P4-BG compared to polymer only controls. Importantly, their findings demonstrate that the pro-angiogenic effect is preserved when BG particles are embedded within a polymer matrix and enabled gradual ion release. Likewise, hypoxia-mimicking strategies have also been reported to enhance vascular pattern formation in PCL-based constructs [7] supporting the sensitivity of this assay to distinct pro-angiogenic stimuli.

Taken together, these findings suggest that angiogenic stimulations in polymer-BG composite systems are not strictly dependent on the presence or absence of phosphorus in the BG composition. Rather, the enhanced VEGFA secretion and endothelial organization observed for the PCL/BG-WS and PCL/BG-YS composite scaffolds are consistent with angiogenic responses previously reported for both phosphorous containing 45S5 and S53P4-based systems, supporting the notion that ion release dynamics and composition-dependent dissolution kinetics play a central role in mediating angiogenoc effects irrespective of phosphorous content.

3.5. Osteogenic properties

To evaluate the osteogenic properties of the developed PCL/BG scaffolds, the expression of osteogenic gene markers (Fig. 5, Fig. S6), ALP activity (Fig. 6A), collagen production (Fig. 6B), and ECM formation (Fig. 6C and D) were assessed in hMSCs cultured directly on the investigated scaffolds after 7 and 28 days.

At day 7 in basic medium, *RUNX2* showed the highest expression, with significant upregulation on PCL/BG-WS and PCL/BG-YS (fold change values of 4.55 ± 0.70 and 5.19 ± 0.56, respectively) than on PCL scaffolds (Fig. 5). Culture in the osteogenic medium resulted in a similar expression pattern and values. (Fig. S6). The approximately 5-fold upregulation of *RUNX2* in both basic and osteogenic media suggests a strong intrinsic effect of both BGs on early osteogenic differentiation, independent of external biochemical stimulation. In contrast, Font Telado et al. reported that PCL scaffolds comprising 10% w/w 52S-BG (a BG from the same glass system as those explored in this study) did not induce significant *RUNX2* upregulation [19]. Similarly, Distler et al. [45] found no notable influence on *RUNX2* expression in PLA scaffolds incorporating 1% w/w benchmark 45S5-BG. Similarly, Mahdavi et al. [52] also found no differences in *RUNX2* gene expression on day 7 in their study investigating electrospun PLGA-scaffolds coated in 1% w/v solution of nano-45S5 BG composites but they did report upregulation of this gene on day 14. These previous findings suggest that low BG content may not result in sufficient ion availability at the cell-material interface to stimulate early osteogenic commitment, regardless of the presence or absence of P_2O_5 in the BG composition. Supporting this dose-dependent effect, Aguilar-Perez et al. [53] reported significant early *RUNX2* upregulation on segmented polyurethane films only at high custom nanoBG (SiO_2–CaO–P_2O_5) content (15-25%) highlighting the importance of BG availability and ion release kinetics for initiating osteogenic differentiation. In line with these observations, Łukowicz et al. [54] reported that P_2O_5-containing sol-gel BGs induced markedly lower early *RUNX2* expression than P_2O_5-free compositions in hMSCs cultured on PLGA composite films, an effect attributed to differences in BG network structure and ion release behavior. Furthermore, Söhling et al. [55] and Wang et al. [9] incorporated 20%w/w of the commercially available S53P4-BG, the same amount as used in this study, into PLA and PCL scaffolds, respectively, yet neither reported significant *RUNX2* upregulation. The surface treatment performed on our scaffolds, absent in the studies of Söhling et al. and Wang et al. likely enhanced BG exposure and subsequent ion release, potentially enhancing the observed osteogenic response.

Interestingly, *ALPL* expression was the highest on day 28 in the case of PCL/BG-WS, with a fold change of 4.25 ± 0.37 (Fig. 5). In contrast, in osteogenic medium, *ALPL* expression was downregulated on composites in comparison with PCL alone at both evaluated time points (Fig. S6). This notably higher *ALPL* expression observed for PCL/BG-WS may be partially explained by the higher Ti content in BG-WS. Ti^{4+} ions have previously been reported to positively influence osteogenic differentiation and specifically enhance *ALPL* gene expression [56,57]. Nevertheless, as discussed earlier, the measured cumulative release of Ti^{4+} ions was comparable between the composites and remained within the trace element range. The low release of Ti from the scaffolds was expected, as it is present in the BG only in trace amounts and the quantifications were performed on composite scaffolds containing 20 wt% BGs dispersed within the polymer matrix. Although the cumulative Ti^{4+} release from both composites was minimal and comparable, Ti may still exert a local effect at the material interface, as previously reported to increase viability and facilitate greater attachment of MC3T3 osteoblasts [36].

At the protein level (Fig. 6A), ALP activity was overall significantly higher on PCL scaffolds compared to both composites, and the same pattern was observed under osteogenic conditions (Fig. S8). A similar response has been reported in other polymer-BG systems, including both the benchmark 45S5 formulations as well as the commercially available S53P4 composition, underscoring that this phenomenon is not unique to the present BG system. For instance, Wang et al. [9] investigated PCL/S53P4 BG composites and observed that ALP activity decreased with increasing BG content, with the highest enzymatic activity detected on PCL alone. Importantly, context-dependent behaviour has also been reported for 45S5-based systems. Poh et al. [58] showed that increased ALP activity was evident only in the presence of osteogenic medium, suggesting that dissolution ion concentrations alone may be insufficient to autonomously induce ALP activity at 10 wt% BG content. In polymer-BG composite systems incorporating conventional 45S5 BG, earlier ALP activation is frequently reported, particularly when BG particles are surface coated rather than embedded within the bulk polymer [9]. For example, Mahdavi et al. [52] observed increased ALP activity at days 7 and 14 in electrospun PLGA scaffolds coated with 1% w/v solution of the nano-45S5 BG, suggesting that rapid ion release from surface-deposited particles induces early osteogenic signalling. Similarly, Yang et al. [59] reported enhanced ALP activity as early as 48 h in PDLLA/45S5 BG composites, with higher activity at 5% BG compared to 40%, which they attributed to excessive ion release and alkalization at higher concentrations. Pádua et al. [60] further demonstrated that ALP activity in 45S5-based composites was concentration dependent and was increased in the presence of dopants such as Zn, Nb. These studies collectively indicate that early robust ALP activation is typically associated with high phosphorous content and rapid ion release kinetics.

In this study, however, the delayed *ALPL* expression alongside the generally higher ALP activity detected on PCL scaffolds, may be explained by the notably low phosphorous content of the investigated BG formulations relative to conventional 45S5 and S53P4 compositions. It is well-established that a high inorganic phosphate concentration significantly induces ALP activation [61,62]. Consequently, the required threshold concentration for activating *ALPL* expression may have been reached only at later time points. Thus, the limited potency of the specific BG formulation in driving *ALPL* expression at both gene and protein levels can likely be attributed to its inherently low phosphorus content.

Regarding the expression of late osteogenic markers, *COL1A1* and *OCN*, which both contribute to matrix formation, several differences were observed (Fig. 5). Expression of *COL1A1* on day 7 was comparable among all conditions. On day 28, however, it was significantly higher on PCL/BG-WS (fold change 2.17 ± 0.27) than in the case of the other two scaffolds. *OCN* increased significantly between day 7 and day 28 on PCL/BG-WS. On day 28, the fold gene expression on PCL/BG-WS reached 3.52 ± 0.10. Culture with osteogenic medium (Fig. S6) resulted in a similar expression pattern of *COL1A1,* while the expression of *OCN* was similar on day 7 but downregulated on day 28 in comparison to PCL.

These results reinforce that both the amount of BGs and the release rate in composite scaffolds influences osteogenic outcomes. Importantly, this dose-dependent behavior has also been described for established

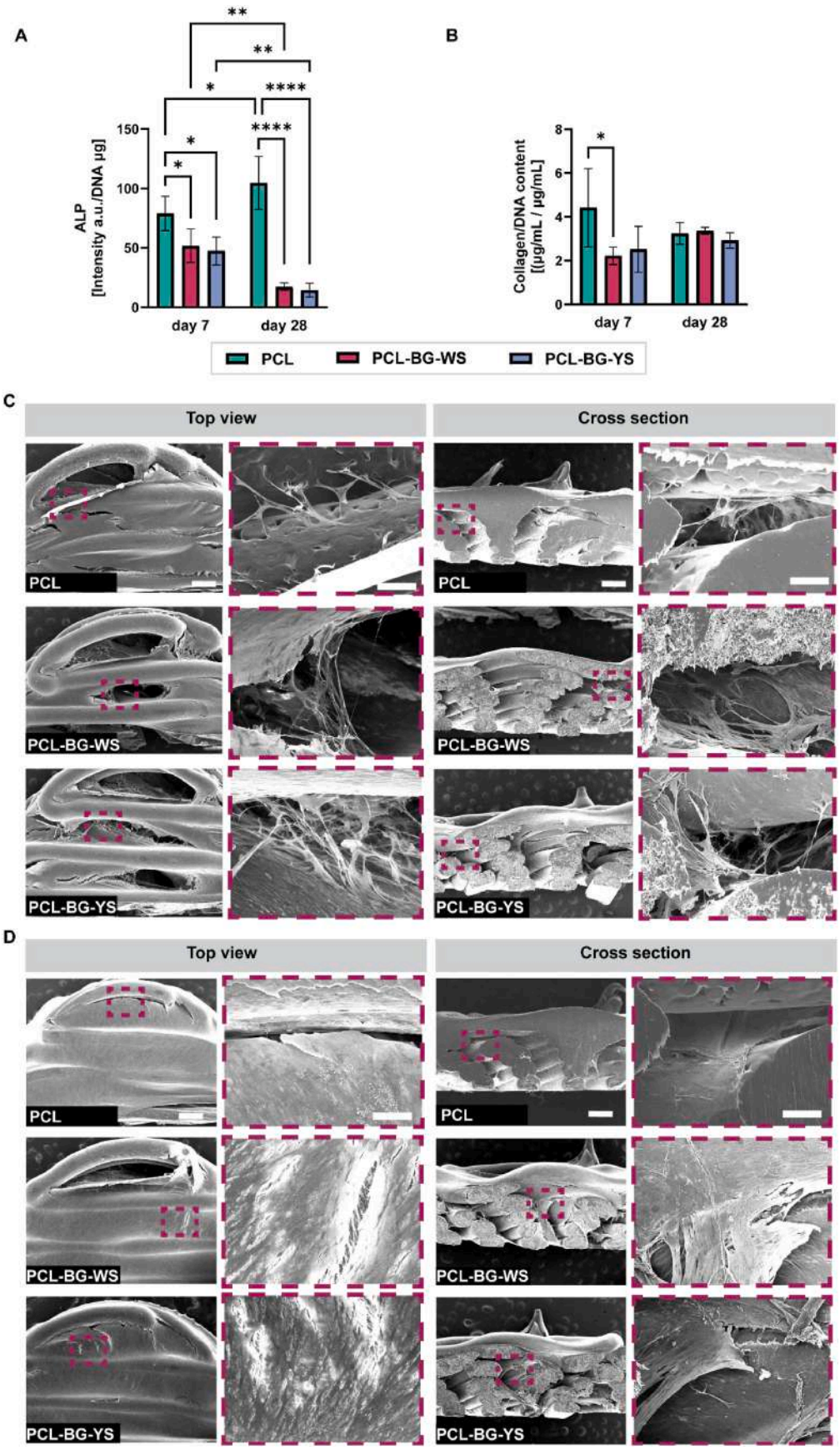

Fig. 6. Osteogenic properties of the scaffolds. (**A**) ALP activity, (**B**) collagen production, ECM formation on (**C**) day 7 and (**D**) day 28 in basic culture medium. Scale bars = 500 µm and 100 µm for the magnified pictures. Levels of statistical significance are indicated by * $p \leq 0.05$, ** $p \leq 0.01$, *** $p \leq 0.001$ and **** $p \leq 0.0001$. Data represents n = 3 biological replicates from one independent experiment.

benchmark and commercially available BGs. Poh et al. [63], using PCL scaffolds incorporating 50 wt% of 45S5 BG reported a significant increase of *OCN* expression after 21 days in basic medium. The high BG loading in that system likely resulted in substantial ion availability necessary to stimulate late osteogenic markers. In contrast, studies employing lower BG content or systems characterized by slower ion release profiles did not consistently demonstrate enhanced stimulatory effect on *OCN* and *COL1A1* expression. For example, Wang et al. [9], investigating PCL/S53P4 composites, observed no clear enhancement of late osteogenic markers compared to polymer controls, indicating that commercially available S53P4 does not uniformly promote late-stage differentiation in a composite form. Similarly, Söhling et al. [55] reported that increasing BG content up to 20% is PLA/S53P4-BG had only a slight effect on osteogenic gene expression, despite improved bioactivity and cell adherence. Distler and co-workers [45], as well as other polymer/BG systems with moderate BG incorporation, also described limited stimulatory effect of *COL1A1* and *OCN* expression under comparable conditions. Notably, Font-Telado et al. [19], using the same BG formulation as in the present study but at a lower concentration (10 wt %), did not observe pronounced upregulation of late osteogenic markers, further underscoring the importance of the BG fraction in reaching biologically effective ion concentrations. Taken together, these data indicate that late osteogenic marker expression does not directly correlate with the mere presence of BG, but rather depends on achieving a composition and dose-dependent ion availability sufficient to sustain matrix maturation.

Finally, ECM formation was investigated and reported in Fig. 6C–D. SEM images of scaffolds cultured with hMSCs for 7 or 28 days revealed matrix production on the top as well as in the cross-section of all three formulations of the scaffolds at both investigated time points. It could be observed that the amount of matrix increased between days 7 and 28 on all scaffold compositions and no particular morphological differences were observed between PCL and PCL/BG-WS, or PCL/BG-YS. Similar observations were made when hMSCs were cultured on scaffolds in osteogenic medium (Fig. S9). On a protein level, the total production of collagen was the highest at day 7 in the case of cultures on PCL scaffolds, while no differences were observed at day 28 (Fig. 6B). These results suggest that all scaffolds supported sufficient matrix deposition. Based on the genetic evaluation (such as *COL1A1* and *ALPL* being upregulated in PCL/BG-WS at day 28), differences in the biochemical composition of the matrix were anticipated, yet longer culture periods and more extensive biological evaluations may be required in future studies to confirm this.

The differences in osteogenic outcomes observed between PCL/BG-WS and PCL/BG-YS composites may be related, as previously anticipated, to the compositional difference on the trace level elements between the BG-WS and BG-YS. While both BGs were previously synthesized from natural raw materials within the same glass system and at identical PCL:BG ratios, previous analysis revealed that BG-WS contained a higher amount of Ti^{4+} ions, whereas BG-YS was richer in Al and Fe [22]. Ti is known to enhance osteogenic differentiation by promoting *ALPL* gene expression and ECM mineralization, which may explain the upregulation of *ALPL* and *COL1A1* observed in the PCL/BG-WS group [56,57]. This suggests that even subtle compositional differences in

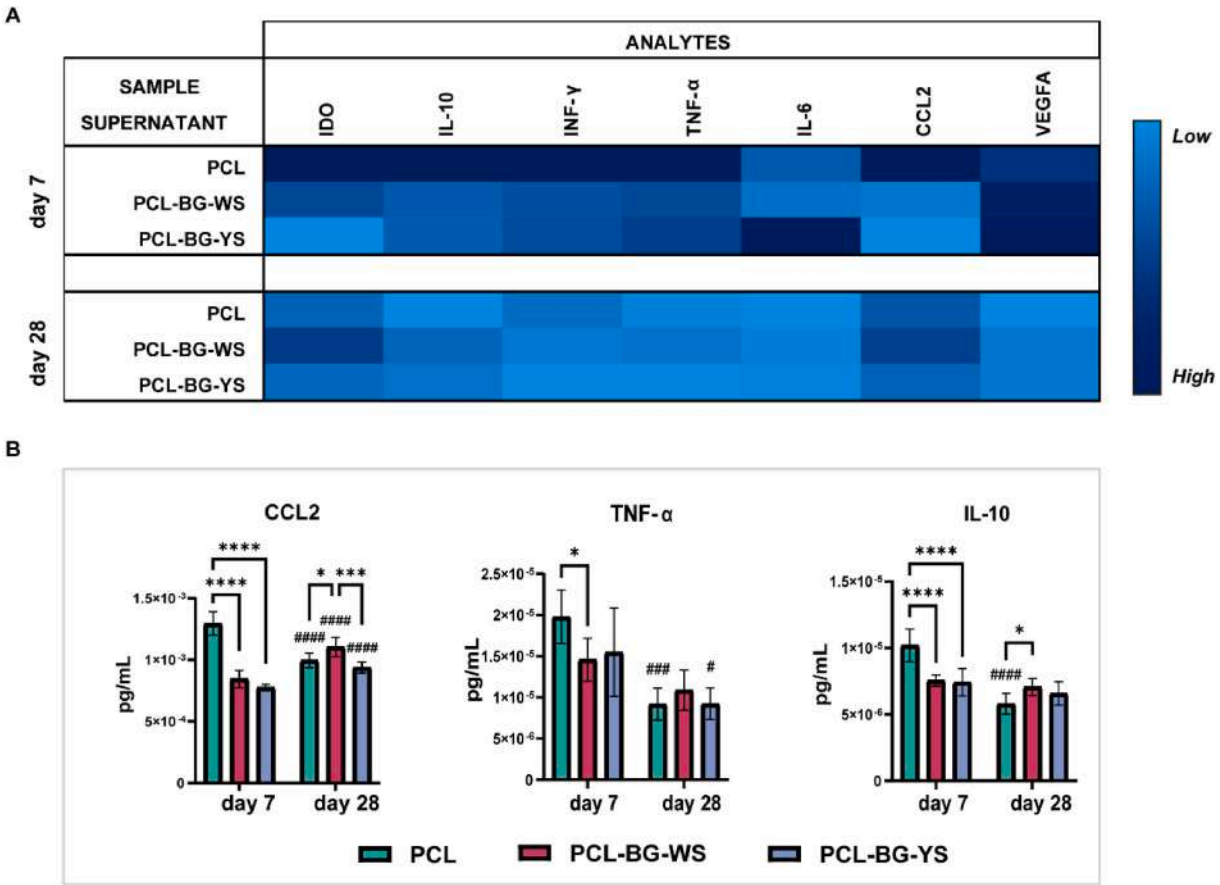

Fig. 7. Influence of the scaffold composition on the paracrine function of hMSCs. (**A**) Heat map demonstrating overall differences in the secretion profiles of hMSCs cultured on different scaffolds (PCL, PCL-BG-WS, and PCL-BG-YS) measured on days 7 and 28. (**B**) Detailed comparison of measured concentrations of CCL2, TNF-α, and IL-10. Symbol # demonstrates the statistical significance of the comparison between days 7 and 28 of the same type of scaffold, while * indicates statistically significant differences between different samples at the same time point. Levels of statistical significance are indicated by * or #p < 0.05, ** or ##p < 0.01, *** or ###p < 0.001 and **** or ####p < 0.0001.

trace elements within otherwise comparable BG systems may significantly affect osteogenic behavior.

3.6. Influence of the scaffold composition on the secretion profile of hMSCs

To study the effect of the added inorganic particles to composite scaffolds on the paracrine function of hMSCs, several pro- and anti-inflammatory cytokines, chemokines, and proteins (Table 2) were measured. The cell culture supernatant of hMSCs cultured on different 3D composites was analyzed using a 10-plex multiplex platform. Fig. 7A shows a heatmap demonstrating the concentrations of measured analytes on days 7 and 28 normalized to the DNA content, while Fig. 7B shows a detailed comparison, including statistical analysis, of the analytes that were expressed the most consistently, including CCL2, TNF-α, IL-10. Furthermore, Fig. S10 shows the cytokine concentrations reflecting a more bioengineering perspective of the cytokine release analysis.

Overall, 7 out of 10 measured analytes were detected in all supernatants. Measured concentrations of IL-1β, MMP-8, and CCL-5 were lower than the lowest concentration on the standard curves for the majority of the samples, and thus outside of the detection range. Of note, the lowest detectable concentration for IL-1β was 1.6 pg/mL, for MMP-8 was 20 pg/mL, and for CCL-5 was 0,6 pg/mL.

The highest concentrations of the measured analytes were detected in supernatants collected after 7 days of hMSCs cultured on PCL scaffolds. Here, the concentrations of CCL2, TNF-a and IL-10 were significantly higher on day 7 than on day 28 (Fig. 7B). In contrast, for the composite scaffolds, the concentrations increased between day 7 and 28 or remained constant. For instance, CCL2 was significantly higher after 28 days for both PCL/BG-WS and PCL/BG-YS composites, while IL-10 remained constant. The cytokine concentrations prior DNA normalization (Fig. S10) followed the same general trend.

These results suggest that on day 7 PCL scaffolds might have triggered inflammatory responses of hMSCs more than the PCL/BG composite scaffolds, while the addition of both BG-WS and BG-YS contributed to reducing the secretion of inflammatory factors. Moreover, the composite scaffolds enhanced the production of pro-angiogenic factors such as CCL2 and the previously mentioned VEGFA. Similar observations were previously reported by Söhling et al. [55], although they employed a different experimental setup using a whole-blood stimulation assay.

Overall, the results of this study demonstrated that both PCL/BG-WS and PCL/BG-YS possess osteogenic, angiogenic, and potential immunomodulatory properties. The composition of the BGs certainly played a crucial role in influencing the biological performance of the composite scaffolds. PCL/BG-WS exhibited the strongest osteogenic responses among the tested formulations, which may be related to its higher content of Ti^{4+} ions compared to BG-YS.

In this study, both composites contained P_2O_5-free BG powders based on the SiO_2–CaO–Na_2O system, which were already reported to have osteogenic and angiogenic properties when directly incubated with hMSCs [18]. Here, we demonstrated that also the incorporation of P_2O_5-free bioactive glasses into a PCL matrix led to enhanced osteogenesis and angiogenesis while potentially modulating inflammatory responses. This highlights the potential of these composite materials for bone tissue engineering.

While this study focused on naturally derived P_2O_5-free BG combined with a polymer, it is important to interpret these findings within the broader context of conventional P_2O_5-containing systems. Most commercially available BGs, such as those based on the 45S5 and S53P4 compositions, contain P_2O_5. Numerous studies have demonstrated that P_2O_5-containing BGs exhibit high bioactivity but may degrade rapidly, which may limit the long-term stability and sustained biological activity of composite designed to improve chemical stability and increase the control of ions release, expanding the landscape of BGs for bone regeneration [19,22]. In this context, the naturally derived P_2O_5-free formulations investigated here (BG-WS and BG-YS) maintained their biological effectiveness when incorporated into PCL while providing a potentially more gradual dissolution profile. The P_2O_5-free BGs can complement or provide sustainable alternatives to the existing BGs and BG-based composites for bone regeneration applications. Importantly, both phosphorous -containing and phosphorous -free BGs have been reported to exhibit osteogenic and angiogenic properties, not only when investigated as BG particles but also, more recently, when incorporated into polymeric matrices as composites. Research on established BG systems, including 45S5 and S53P4 formulations, demonstrates that their incorporation into biodegradable polymer scaffolds supports regenerative responses relevant for bone repair. Similarly, emerging P_2O_5-free systems have shown promising biological performance, supporting the notion that the biological responses are likely governed by ion release dynamics and compositional tuning rather than solely by the presence or absence of phosphorous. Within this broader framework, the present study contributes an example of P_2O_5-free polymer-BG composites that maintains osteogenic and angiogenic functionality while offering an alternative compositional strategy for scaffold design.

In conclusion, further investigations should be conducted that include direct co-cultures of hMSCs (or osteoprogenitor cells) and HUVECs on the PCL/BG-WS scaffolds. It would be valuable to understand how cell-to-cell interactions influence osteogenic and angiogenic responses with respect to the composite scaffolds, enabling further refinement of scaffold designs for improved bone regeneration, including vascularization. Furthermore, inclusion of hMSCs from multiple donors would be important to account to assess inter-donor variability and to further validate the observed responses across cellular heterogeneity. An assessment of these scaffolds *in vivo*, in injury models where a good vascularization is of utmost importance, should be considered as an ultimate step to evaluate the translational potential of this composite-based scaffold. In addition, future studies should address the role of the polymer-BG interface on the degradation behaviour and the time-dependent evolution of mechanical properties during BG dissolution, which are particularly relevant for load-bearing applications but were outside the scope of the present work.

4. Conclusion

This study demonstrates that the presence of bioactive glasses with tailored trace element composition in composite materials enhances the osteogenic and angiogenic properties of the scaffolds. This was reflected by the upregulated expression of early and late osteogenic markers as well as enhanced matrix deposition. Additionally, the composites stimulated the secretion of pro-angiogenic factors, while limiting inflammatory processes, in comparison with PCL only scaffolds. The developed composite materials, here successfully fabricated into an additive manufactured 3D scaffold, represent a promising advancement in bone substitute materials, offering new potential for enhanced bone regeneration and improved outcomes in tissue engineering. Future investigations should focus on long-term *in vivo* validation and optimization of BG composition to further enhance regenerative outcomes.

CRediT authorship contribution statement

Martyna Nikody: Conceptualization, Formal analysis, Investigation, Methodology, Writing – original draft, Writing – review & editing. **Sophia Dalfino:** Conceptualization, Formal analysis, Investigation, Methodology, Writing – original draft, Writing – review & editing. **Pamela Habibovic:** Funding acquisition, Resources, Supervision, Writing – review & editing. **Lizette Morejón:** Formal analysis, Methodology, Resources, Writing – review & editing. **José A. Delgado:** Formal analysis, Methodology, Resources, Writing – review & editing. **Gianluca Martino Tartaglia:** Conceptualization, Funding acquisition,

Resources, Supervision, Writing – review & editing. **Claudia Dolci:** Formal analysis, Resources, Supervision, Writing – review & editing. **Elizabeth R. Balmayor:** Conceptualization, Formal analysis, Supervision, Writing – review & editing. **Lorenzo Moroni:** Conceptualization, Formal analysis, Resources, Supervision, Writing – review & editing.

Declaration of competing interest

The authors declare that they have no known competing financial interests or personal relationships that could have appeared to influence the work reported in this paper.

Appendix A. Supplementary data

Supplementary data to this article can be found online at https://doi.org/10.1016/j.biomaterials.2026.124325.

Data availability

Data will be made available on request.

References

[1] H.R. Fernandes, A. Gaddam, A. Rebelo, D. Brazete, G.E. Stan, J.M.F. Ferreira, Bioactive glasses and glass-ceramics for healthcare applications in bone regeneration and tissue engineering, Materials 11 (2018), https://doi.org/10.3390/ma11122530. Basel.

[2] N. Xue, X. Ding, R. Huang, R. Jiang, H. Huang, X. Pan, W. Min, J. Chen, J.A. Duan, P. Liu, Y. Wang, Bone tissue engineering in the treatment of bone defects, Pharmaceuticals 15 (2022), https://doi.org/10.3390/ph15070879.

[3] M.N. Rahaman, D.E. Day, B. Sonny Bal, Q. Fu, S.B. Jung, L.F. Bonewald, A. P. Tomsia, Bioactive glass in tissue engineering, Acta Biomater. 7 (2011) 2355–2373, https://doi.org/10.1016/J.ACTBIO.2011.03.016.

[4] A. Martelli, D. Bellucci, V. Cannillo, Additive manufacturing of polymer/bioactive glass scaffolds for regenerative medicine: a review, Polymers 15 (2023), https://doi.org/10.3390/POLYM15112473.

[5] F. Baino, S. Hamzehlou, S. Kargozar, Bioactive glasses: where are we and where are we going? J. Funct. Biomater. 9 (2018) https://doi.org/10.3390/JFB9010025.

[6] L.L. Hench, I. Thompson, Twenty-first century challenges for biomaterials, J. R. Soc. Interface 7 (2010), https://doi.org/10.1098/RSIF.2010.0151.FOCUS.

[7] Y. Yan, H. Chen, H. Zhang, C. Guo, K. Yang, K. Chen, R. Cheng, N. Qian, N. Sandler, Y.S. Zhang, H. Shen, J. Qi, W. Cui, L. Deng, Vascularized 3D printed scaffolds for promoting bone regeneration, Biomaterials (2019) 190–191, https://doi.org/10.1016/J.BIOMATERIALS.2018.10.033, 97–110.

[8] W. Wang, L. Wang, B. Zhang, S. Shang, C. Zhao, W. Zhang, J. Chen, C. Zhou, H. Zhou, S. Feng, 3D printing of personalized magnesium composite bone tissue engineering scaffold for bone and angiogenesis regeneration, Chem. Eng. J. 484 (2024) 149444, https://doi.org/10.1016/J.CEJ.2024.149444.

[9] X. Wang, B.Z. Molino, S. Pitkänen, M. Ojansivu, C. Xu, M. Hannula, J. Hyttinen, S. Miettinen, L. Hupa, G. Wallace, 3D scaffolds of Polycaprolactone/copper-Doped bioactive glass: architecture engineering with additive manufacturing and cellular assessments in a coculture of bone marrow stem cells and endothelial cells, ACS Biomater. Sci. Eng. 5 (2019) 4496–4510, https://doi.org/10.1021/ACSBIOMATERIALS.9B00105.

[10] L. Xia, W. Ma, Y. Zhou, Z. Gui, A. Yao, D. Wang, A. Takemura, M. Uemura, K. Lin, Y. Xu, Stimulatory effects of boron containing bioactive glass on osteogenesis and angiogenesis of polycaprolactone: in vitro Study, Biomed Res. Int. 2019 (2019), https://doi.org/10.1155/2019/8961409.

[11] L.L. Hench, J.R. Jones, Bioactive glasses: frontiers and challenges, Front. Bioeng. Biotechnol. 3 (2015), https://doi.org/10.3389/FBIOE.2015.00194.

[12] J.R. Jones, Review of bioactive glass: from hench to hybrids, Acta Biomater. 9 (2013) 4457–4486, https://doi.org/10.1016/J.ACTBIO.2012.08.023.

[13] M. Cannio, D. Bellucci, J.A. Roether, D.N. Boccaccini, V. Cannillo, Bioactive glass applications: a literature review of human clinical trials, Materials 14 (2021), https://doi.org/10.3390/MA14185440.

[14] A. Hoppe, N.S. Güldal, A.R. Boccaccini, A review of the biological response to ionic dissolution products from bioactive glasses and glass-ceramics, Biomaterials 32 (2011) 2757–2774, https://doi.org/10.1016/J.BIOMATERIALS.2011.01.004.

[15] S. Kargozar, F. Baino, S. Hamzehlou, R.G. Hill, M. Mozafari, Bioactive glasses: sprouting angiogenesis in tissue engineering, Trends Biotechnol. 36 (2018) 430–444, https://doi.org/10.1016/j.tibtech.2017.12.003.

[16] F. Döhler, A. Mandlule, L. Van Wüllen, M. Friedrich, D.S. Brauer, 31 P NMR characterisation of phosphate fragments during dissolution of calcium sodium phosphate glasses, J. Mater. Chem. B 3 (2015) 1125–1134, https://doi.org/10.1039/C4TB01757A.

[17] M.H. Kaou, M. Furkó, K. Balázsi, C. Balázsi, Advanced bioactive glasses: the newest achievements and breakthroughs in the area, Nanomaterials 13 (2023) 2287, https://doi.org/10.3390/NANO13162287.

[18] M. Nikody, L. Kessels, M. Schumacher, P. Habibovic, In vitro osteogenic and in ovo angiogenic effects of a family of natural origin P2O5-free bioactive glasses, RSC Adv. 14 (2024) 34708–34717, https://doi.org/10.1039/D4RA04731A.

[19] S. Font Tellado, J.A. Delgado, S.P.P. Poh, W. Zhang, M. Garcia-Valles, S. Martinez, A. Gorustovich, L. Morejon, M. Van Griensven, E.R. Balmayor, Phosphorous pentoxide-free bioactive glass exhibits dose-dependent angiogenic and osteogenic capacities which are retained in glass polymeric composite scaffolds, Biomater. Sci. 9 (2021) 7876–7894, https://doi.org/10.1039/d1bm01311d.

[20] M. Suárez, E. Fernández-García, A. Fernández, R. López-Píriz, R. Díaz, R. Torrecillas, Novel antimicrobial phosphate-free glass–ceramic scaffolds for bone tissue regeneration, Sci. Rep. 10 (2020), https://doi.org/10.1038/s41598-020-68370-y.

[21] J.R. Jones, O. Tsigkou, E.E. Coates, M.M. Stevens, J.M. Polak, L.L. Hench, Extracellular matrix formation and mineralization on a phosphate-free porous bioactive glass scaffold using primary human osteoblast (HOB) cells, Biomaterials 28 (2007) 1653–1663, https://doi.org/10.1016/j.biomaterials.2006.11.022.

[22] L.M. Alonso, J.Á.D. García-Menocal, M. García-Vallés, S.M. Manent, E.R. Balmayor, M. van Griensven, Exploring the use of silica sands and calcite from natural deposits to prepare bioactive glasses, Int. J. Mater. Res. 110 (2018) 333–342, https://doi.org/10.3139/146.111716.

[23] M. Cámara-Torres, P. Fucile, R. Sinha, C. Mota, L. Moroni, Boosting bone regeneration using augmented melt-extruded additive-manufactured scaffolds, Int. Mater. Rev. 68 (2023) 755–785, https://doi.org/10.1080/09506608.2022.2153219/ASSET/IMAGES/LARGE/10.1080_09506608.2022.2153219-FIG6.JPEG.

[24] S. Dalfino, E. Olaret, M. Piazzoni, P. Savadori, I. Stancu, G. Tartaglia, C. Dolci, L. Moroni, Polycaprolactone/β-Tricalcium phosphate composite scaffolds with advanced pore geometries promote human mesenchymal stromal cells' osteogenic differentiation, Tissue Eng. (2024), https://doi.org/10.1089/ten.tea.2024.0030.

[25] R. Sinha, M. Cámara-Torres, P. Scopece, E. Verga Falzacappa, A. Patelli, L. Moroni, C. Mota, A hybrid additive manufacturing platform to create bulk and surface composition gradients on scaffolds for tissue regeneration, Nat. Commun. 12 (2021), https://doi.org/10.1038/s41467-020-20865-y.

[26] A. Sensini, C. Gualandi, M.L. Focarete, J. Belcari, A. Zucchelli, L. Boyle, G.C. Reilly, A.P. Kao, G. Tozzi, L. Cristofolini, Multiscale hierarchical bioresorbable scaffolds for the regeneration of tendons and ligaments, Biofabrication 11 (2019), https://doi.org/10.1088/1758-5090/ab20ad.

[27] A.M. Martins, Q.P. Pham, P.B. Malafaya, R.A. Sousa, M.E. Gomes, R.M. Raphael, F. K. Kasper, R.L. Reis, A.G. Mikos, The role of lipase and α-amylase in the degradation of starch/poly(Caprolactone) fiber meshes and the osteogenic differentiation of cultured marrow stromal cells, Tissue Eng. 15 (2009) 295–305, https://doi.org/10.1089/ten.tea.2008.0025.

[28] E.R. Balmayor, K. Tuzlakoglu, A.P. Marques, H.S. Azevedo, R.L. Reis, A novel enzymatically-mediated drug delivery carrier for bone tissue engineering applications: combining biodegradable starch-based microparticles and differentiation agents, J. Mater. Sci. Mater. Med. (2008) 1617–1623, https://doi.org/10.1007/s10856-008-3378-5.

[29] J.L. Dávila, M.S. Freitas, P. Inforçatti Neto, Z.C. Silveira, J.V.L. Silva, M.A. D'Ávila, Fabrication of PCL/β-TCP scaffolds by 3D mini-screw extrusion printing, J. Appl. Polym. Sci. 133 (2016), https://doi.org/10.1002/app.43031.

[30] T.T. Swe, H. Mohamad, K.A. Shariff, A.F.M. Noor, K. Ishikawa, A.A. Thant, Synthesis and characterization of bioactive Quaternary silicate gel-glasses, in: J. Phys. Conf. Ser., Institute of Physics Publishing, 2018, https://doi.org/10.1088/1742-6596/1082/1/012070.

[31] A. Di Luca, I. Lorenzo-Moldero, C. Mota, A. Lepedda, D. Auhl, C. Van Blitterswijk, L. Moroni, Tuning cell differentiation into a 3D scaffold presenting a pore shape gradient for osteochondral regeneration, Adv. Healthcare Mater. 5 (2016) 1753–1763, https://doi.org/10.1002/adhm.201600083.

[32] M. Cámara-Torres, R. Sinha, A. Sanchez, P. Habibovic, A. Patelli, C. Mota, L. Moroni, M. Cámara-Torres, R. Sinha, P. Habibovic, C. Mota, L. Moroni, A. Sánchez, A. Patelli, Effect of highly loaded nanohydroxyapatite composite scaffolds prepared via melt extrusion additive manufacturing on the osteogenic differentiation of human mesenchymal stromal cells, (n.d.). https://doi.org/10.1101/2021.01.21.427568.

[33] C. Wang, C. Meng, Z. Zhang, Q. Zhu, 3D printing of polycaprolactone/bioactive glass composite scaffolds for in situ bone repair, Ceram. Int. 48 (2022) 7491–7499, https://doi.org/10.1016/j.ceramint.2021.11.293.

[34] A.R.C. Duarte, J.F. Mano, R.L. Reis, Enzymatic degradation of 3D scaffolds of starch-poly-(ε-caprolactone) prepared by supercritical fluid technology, Polym. Degrad. Stabil. 95 (2010) 2110–2117, https://doi.org/10.1016/j.polymdegradstab.2010.06.020.

[35] J. Turner, A. Nandakumar, N. Anilbhai, A.R. Boccaccini, J.R. Jones, G. Jell, The effect of Si species released from bioactive glasses on cell behaviour: a quantitative review, Acta Biomater. 170 (2023) 39–52, https://doi.org/10.1016/j.actbio.2023.09.012.

[36] L.M. Placek, T.J. Keenan, Y. Li, C. Yatongchai, D. Pradhan, D. Boyd, N.P. Mellott, A. W. Wren, Investigating the effect of TiO2 on the structure and biocompatibility of bioactive glass, J. Biomed. Mater. Res. B Appl. Biomater. 104 (2016) 1703–1712, https://doi.org/10.1002/JBM.B.33521.

[37] T. Zhou, Z. Xu, H. Sun, A.M. Beltrán, Q. Nawaz, B. Sui, A.R. Boccaccini, K. Zheng, Unlocking the potential of iron-containing mesoporous bioactive glasses: orchestrating osteogenic differentiation in bone marrow mesenchymal stem cells and osteoblasts, Colloids Surf. A Physicochem. Eng. Asp. 694 (2024), https://doi.org/10.1016/J.COLSURFA.2024.134188.

[38] D.S. Brauer, Bioaktive Gläser: struktur und Eigenschaften, Angew. Chem. 127 (2015) 4232–4254, https://doi.org/10.1002/ange.201405310.

[39] J. Ródenas-Rochina, J.L.G. Ribelles, M. Lebourg, Comparative study of PCL-HAp and PCL-Bioglass composite scaffolds for bone tissue engineering, J. Mater. Sci. Mater. Med. 24 (2013) 1293–1308, https://doi.org/10.1007/s10856-013-4878-5.
[40] S. Midha, T.B. Kim, W. Van Den Bergh, P.D. Lee, J.R. Jones, C.A. Mitchell, Preconditioned 70S30C bioactive glass foams promote osteogenesis in vivo, Acta Biomater. 9 (2013) 9169–9182, https://doi.org/10.1016/j.actbio.2013.07.014.
[41] G. Carpentier, S. Berndt, S. Ferratge, W. Rasband, M. Cuendet, G. Uzan, & Patricia Albanese, Angiogenesis Analyzer for imageJ-A comparative morphometric analysis of "endothelial tube formation Assay" and "fibrin Bead Assay," (n.d.). https://doi.org/10.1038/s41598-020-67289-8.
[42] I. Arnaoutova, H.K. Kleinman, In vitro angiogenesis: endothelial cell tube formation on gelled basement membrane extract, Nat. Protoc. 5 (2010) 628–635, https://doi.org/10.1038/nprot.2010.6.
[43] K. Dashnyam, A. El-Fiqi, J.O. Buitrago, R.A. Perez, J.C. Knowles, H.W. Kim, A mini review focused on the proangiogenic role of silicate ions released from silicon-containing biomaterials, J. Tissue Eng. 8 (2017), https://doi.org/10.1177/2041731417707339/ASSET/0C50C69D-8A09-4EEC-8AAF-FB7B40CA9DBE/ASSETS/IMAGES/LARGE/10.1177_2041731417707339-FIG6.JPG.
[44] P. Sutthavas, M. Schumacher, M. Nikody, V. Ramesh, J. Jakobi, E.R. Balmayor, P. Habibovic, C. Rehbock, S. Barcikowski, S. van Rijt, Laser-based ion doping is a suitable alternative to dope biologically active ions into colloidal bioglass nanoparticles, Mater. Adv. (2023), https://doi.org/10.1039/D3MA00112A.
[45] T. Distler, N. Fournier, A. Grünewald, C. Polley, H. Seitz, R. Detsch, A. R. Boccaccini, Polymer-bioactive glass composite filaments for 3D scaffold manufacturing by fused deposition modeling: fabrication and characterization, Front. Bioeng. Biotechnol. 8 (2020), https://doi.org/10.3389/FBIOE.2020.00552.
[46] J. Wu, Z. Wu, Z. Xue, H. Li, J. Liu, PHBV/bioglass composite scaffolds with co-cultures of endothelial cells and bone marrow stromal cells improve vascularization and osteogenesis for bone tissue engineering, RSC Adv. 7 (2017) 22197–22207, https://doi.org/10.1039/c7ra02767b.
[47] G. Strömberg, L. Aalto-Setälä, P. Uppstu, R. Björkenheim, J. Pajarinen, E. Eriksson, N.C. Lindfors, L. Hupa, Development and characterization of non-coated and PLGA-coated S53P4 and S59 bioactive glass scaffolds for treatment of load-bearing defects, Biomed. Mater. Devices 2 (1 2) (2023) 498–509, https://doi.org/10.1007/s44174-023-00099-4, 2023.
[48] L.C. Gerhardt, K.L. Widdows, M.M. Erol, C.W. Burch, J.A. Sanz-Herrera, I. Ochoa, R. Stämpfli, I.S. Roqan, S. Gabe, T. Ansari, A.R. Boccaccini, The pro-angiogenic properties of multi-functional bioactive glass composite scaffolds, Biomaterials 32 (2011) 4096–4108, https://doi.org/10.1016/J.BIOMATERIALS.2011.02.032.
[49] R.M. Day, V. Maquet, A.R. Boccaccini, R. Jérôme, A. Forbes, In vitro and in vivo analysis of macroporous biodegradable poly(D,L-lactide-co-glycolide) scaffolds containing bioactive glass, J. Biomed. Mater. Res. 75 (2005) 778–787, https://doi.org/10.1002/jbm.a.30433.
[50] H. Keshaw, G. Georgiou, J.J. Blaker, A. Forbes, J.C. Knowles, R.M. Day, Assessment of polymer/bioactive glass-composite microporous spheres for tissue regeneration applications, Tissue Eng. 15 (2009) 1451–1461, https://doi.org/10.1089/ten.tea.2008.0203.
[51] S. Cichos, E. Schätzlein, N. Wiesmann-Imilowski, A. Blaeser, D. Henrich, J. Frank, P. Drees, E. Gercek, U. Ritz, A new 3D-printed polylactic acid-bioglass composite for bone tissue engineering induces angiogenesis in vitro and in ovo, Int. J. Bioprint. 9 (2023), https://doi.org/10.18063/ijb.751.
[52] F.S. Mahdavi, A. Salehi, E. Seyedjafari, A. Mohammadi-Sangcheshmeh, A. Ardeshirylajimi, Bioactive glass ceramic nanoparticles-coated poly(l-lactic acid) scaffold improved osteogenic differentiation of adipose stem cells in equine, Tissue Cell 49 (2017) 565–572, https://doi.org/10.1016/j.tice.2017.07.003.
[53] F.J. Aguilar-Pérez, R.F. Vargas-Coronado, J.M. Cervantes-Uc, J.V. Cauich-Rodríguez, C. Covarrubias, M. Pedram-Yazdani, Preparation and bioactive properties of nano bioactive glass and segmented polyurethane composites, J. Biomater. Appl. 30 (2016) 1362–1372, https://doi.org/10.1177/0885328215626361.
[54] K. Łukowicz, B. Zagrajczuk, A. Nowak, Ł. Niedźwiedzki, M. Laczka, K. Cholewa-Kowalska, A.M. Osyczka, The role of CaO/SiO2 ratio and P2O5 content in gel-derived bioactive glass-polymer composites in the modulation of their bioactivity and osteoinductivity in human BMSCs, Mater. Sci. Eng., C 109 (2020) 110535, https://doi.org/10.1016/j.msec.2019.110535.
[55] N. Söhling, S. Al Zoghool, E. Schätzlein, J. Neijhoft, K.M.C. Oliveira, L. Leppik, U. Ritz, E. Dörsam, J. Frank, I. Marzi, A. Blaeser, D. Henrich, In vitro evaluation of a 20% bioglass-containing 3D printable PLA composite for Bone Tissue Engineering, Int. J. Bioprint. 8 (2022) 65–81, https://doi.org/10.18063/IJB.V8I4.602.
[56] P. Santiago-Medina, P.A. Sundaram, N. Diffoot-Carlo, Titanium oxide: a bioactive factor in osteoblast differentiation, Int. J. Dent. 2015 (2015) 357653, https://doi.org/10.1155/2015/357653.
[57] E.A. Abou Neel, T. Mizoguchi, M. Ito, M. Bitar, V. Salih, J.C. Knowles, In vitro bioactivity and gene expression by cells cultured on titanium dioxide doped phosphate-based glasses, Biomaterials 28 (2007) 2967–2977, https://doi.org/10.1016/j.biomaterials.2007.03.018.
[58] P.S.P. Poh, D.W. Hutmacher, M.M. Stevens, M.A. Woodruff, Fabrication and in vitro characterization of bioactive glass composite scaffolds for bone regeneration, Biofabrication 5 (2013), https://doi.org/10.1088/1758-5082/5/4/045005.
[59] X.B. Yang, D. Webb, J. Blaker, A.R. Boccaccini, V. Maquet, C. Cooper, R.O. C. Oreffo, Evaluation of human bone marrow stromal cell growth on biodegradable polymer/Bioglass® composites, Biochem. Biophys. Res. Commun. 342 (2006) 1098–1107, https://doi.org/10.1016/j.bbrc.2006.02.021.
[60] A.S. Pádua, M.P.F. Graça, J.C. Silva, Polycaprolactone/Doped bioactive glass composite scaffolds for bone regeneration, J. Funct. Biomater. 16 (2025) 1–20, https://doi.org/10.3390/jfb16060200.
[61] G.R. Beck, Inorganic phosphate as a signaling molecule in osteoblast differentiation, J. Cell. Biochem. 90 (2003) 234–243, https://doi.org/10.1002/JCB.10622.
[62] C.F. Dick, A.L.A. Dos-Santos, J.R. Meyer-Fernandes, Inorganic phosphate as an important regulator of phosphatases, Enzym. Res. 2011 (2011) 103980, https://doi.org/10.4061/2011/103980.
[63] P.S.P. Poh, D.W. Hutmacher, B.M. Holzapfel, A.K. Solanki, M.M. Stevens, M. A. Woodruff, In vitro and in vivo bone formation potential of surface calcium phosphate-coated polycaprolactone and polycaprolactone/bioactive glass composite scaffolds, Acta Biomater. 30 (2016) 319–333, https://doi.org/10.1016/j.actbio.2015.11.012.